RSC Publishing Soft Matter

Lysine functionalised amyloid fibrils: the design and assembly of a TTR1-based peptide

Journal:	*Soft Matter*
Manuscript ID:	SM-ART-09-2012-027244.R2
Article Type:	Paper
Date Submitted by the Author:	n/a

Complete List of Authors:	Bongiovanni, Marie; The University of Melbourne, The Bio21 Molecular Science and Biotechnology Institute; The University of Melbourne, Chemical and Biomolecular Engineering Caruso, Frank; The University of Melbourne, Chemical and Biomolecular Engineering Gras, Sally; University of Melbourne, Bio21 Molecular Science and Biotechnology Institute; University of Melbourne, Department of Chemical and Biomolecular Engineering

Soft Matter

Full paper submission

Soft Matter is a new publication from the Royal Society of Chemistry, providing a forum for the communication of generic science underpinning the properties and applications of soft matter.

2011: Impact Factor:
4.39
2011: Immediacy Index:
0.898
www.softmatter.org

The following paper has been submitted to Soft Matter for consideration as a full paper.

Soft Matter aims to publish high quality papers reporting on the generic science underpinning the properties, applications, and phenomena of soft matter. The primary criterion for acceptance of a contribution for publication is that it must report high-quality new science and make a significant contribution to its field. Soft Matter is an interdisciplinary journal and suitable papers should cross disciplines or be highly significant within the field from which they originate.

Routine or incremental work, however competently researched and reported, should not be recommended for publication if it does not meet our expectations with regard to novelty and impact.

Thank you for your effort in reviewing this submission. It is only through the continued service of referees that we can maintain both the high quality of the publication and the rapid response times to authors. We would greatly appreciate if you could review this paper in two weeks. Please let us know if that will not be possible. Please support all comments with scientific justifications or we may be unable to use your report/ask for extra feedback.

Once again, we appreciate your time in serving as a reviewer. To acknowledge this, the RSC offers a 25% discount on its books: http://www.rsc.org/Shop/books/discounts.asp. Please also consider submitting your next manuscript to Soft Matter.

Best wishes,

Liz Davies

Liz Davies
Editor, Soft Matter

Title

Lysine functionalised amyloid fibrils: the design and assembly of a TTR1-based peptide.

Running title

Lysine functionalised amyloid fibrils

Authors

Marie N. Bongiovanni[1,2], Frank Caruso[1] and Sally L. Gras[1,2]

[1]Department of Chemical and Biomolecular Engineering, The University of Melbourne, Parkville, VIC 3010, Australia, and

[2]Bio21 Molecular Science and Biotechnology Institute, The University of Melbourne, Parkville, VIC 3010, Australia.

Abstract

Non-core residues can affect the formation and protofilament packing of fibrils assembled from short peptide sequences. These residues are of interest in understanding amyloid diseases and in the design of self-assembling peptide materials with a cross-β core, where the assembly process should be reproducible and functional groups accessible on the fibril surface. In this study, the well characterised TTR1 peptide, also known as $TTR_{105-115}$, was functionalised with glycine and lysine residues forming the peptide TTR1-GGK, with the aim of producing a self-assembling fibril scaffold that can be functionalised following assembly. A second aim was to develop a sequence capable of fibril assembly under a wide range of solution conditions. The lysine residue was found accessible on the surface of TTR1-GGK fibrils and the C-terminal residues influenced the mature fibril width and rate of fibril assembly, as observed for other TTR1-based fibrils. The assembly of TTR1-GGK fibrils was examined for conditions of varying ionic strength (NaCl, 0 - 0.5 M), solution pH or in the presence of anions (NaCl, NaI, $NaNO_3$ and $NaSO_4$) or cations (NaCl, $CaCl_2$, $MgCl_2$, LiCl and KCl). The addition of salt increased the rate of TTR1-GGK fibril nucleation but decreased the rate of elongation at high salt concentrations. A combination of electrostatic and hydrophobic interactions was found to promote initial contacts between peptides. Specific ion effects were seen with chaotropic anions, which promoted fibril nucleation. The cross-β core structure, secondary structure and morphology of TTR1-GGK fibrils were largely unaltered by the presence of salt or a range of solution pH. The length of fibrils was also maintained at the high ionic strengths tested, indicating that these fibrils may make suitable scaffolds for fibril functionalisation under a range of conditions.

Keywords

Self-assembly, X-ray diffraction, protein folding, FTIR, β-sheet, Hofmeister salts

1. Introduction

Amyloid fibrils share a fibrous morphology and a common internal cross-β core structure.[1] A range of sequences readily form amyloid fibrils, including proteins involved in disease and functional sequences, such as those found in bacterial biofilms.[2] Synthetic peptides can also form amyloid-like fibrils, providing simple systems to study fibril assembly and the possibility of designed β-sheet rich biomaterials.

As a class of materials, amyloid fibrils have notable properties, including stability in denaturing conditions,[3, 4] resistance to mechanical loading,[5, 6] high mechanical strength,[7] stiffness[8] and an elongated morphology. Synthetic peptides can also be designed to display solvent accessible functional groups away from the fibril core,[9, 10] introducing ligands to mediate specific cell interactions[9] or biologically functional enzymes.[11]

Given the substantial interest in the production of peptide-based biomaterials,[12, 13] including synthetic fibrils, methods are needed to control assembly.[14] A challenge posed by the addition of functional sequences, is that small changes in non-core functional residues can alter the kinetics of assembly for each newly designed peptide.[15] Fibril polymorphism can also occur in fibrils from the same sequence assembled under similar solution conditions,[16-19] potentially impacting on the display of functional groups on the fibril surface. The production of a fibril scaffold that can be functionalised following assembly can overcome some of these problems. An improved understanding of the effect of different physiochemical conditions and polypeptide sequence on the formation and structure of fibrils will also assist in the development of more robust processes for the production of fibrillar materials.

Several sequence and physiochemical factors can alter both the rate of amyloid fibril formation and the cross-β core structure within fibrils.[20] Fibril formation is considered independent of primary sequence[1] but the sequence hydrophobicity, β-sheet propensity and electrostatic interactions between residues can alter the rate of fibril formation considerably. The orientation of residue side groups on adjacent β-sheets can also influence core structure or the association of protofibrils within the mature fibril.[21] Among the physiochemical factors that influence fibril formation, the concentration of salt or changes in solution pH have also been well studied for their ability to alter both the kinetics of assembly[22, 23] and alter the orientation of polypeptides within the fibril.[24-27]

Salt ions can influence protein folding, as well as protein solubility and stability in an aqueous solution.[28] Salt can also be used to screen electrostatic repulsion promoting fibril formation. Ion specific effects, typically above ~100 mM, can affect solubility either through their chaotropic (salting a protein in the solution) or kosmotropic (salting a protein out) nature.[28] A chaotropic ion stabilises the hydration layer immediately surrounding the protein, increasing solubility.[28] A kosmotropic ion has the opposite effect, disrupting the hydration layer, leading to a decrease in solubility.[28] The Hofmeister series ranks salt ions for their charotropic or kosmotropic strength, based on precipitation of the protein lysozyme. While the mechanisms responsible for the Hofmeister effect are complex, evidence points to the influence of ion surface polarity and ion surface charge on ion-water interactions.[28, 29] This series of salts is a useful toolbox for exploring and understanding fibril formation.

Several studies have examined the effect of salts on fibril formation. The rates of fibril formation by β-microglobulin,[25] glucagon[30] and the mouse PrP[31] were shown to follow the order of the electroselectivity series, while α-synuclein [32], an amyloidogenic light chain protein (AL-12) [27] and the yeast prion protein Sup35 NM [33] form fibrils at rates consistent with the order of the Hofmeister series. Cation-specific effects can also impact on fibril formation.[34, 35] For example, cation-specific effects have been shown to have a greater impact on the duration of the lag time for β-lactoglobulin fibril formation at low pH than increases in solution ionic strength.[35] In contrast, fibril formation by Amyloid-β(1-40) [24] or amylin[36] correlated with the order of selected salt in both the Hofmeister and electroselectivity series. The presence of salt has also been shown to affect fibril structure as assessed by electron microscopy, infrared spectroscopy circular dichroism spectroscopy and atomic force microscopy.[24, 25, 31,35,37] Notably, the untwisting of β-lactoglobulin fibrils was shown to correlate to a systematic increase in solution ionic strength, indicating that the morphology of these fibrils is govern by electrostatics.[37] These studies show that salt is an important factor to consider when designing functional fibril sequences.

Synthetic peptides based on the TTR1 sequence ($TTR_{105-115}$ or YTIAALLSPYS in single amino acid code) form an interesting family of fibril forming peptides with potential for development as fibrous materials and can provide insights into the role peptide sequence and the physiochemical environment in fibril assembly. The parent TTR1 peptide forms fibrils that have been well characterised by ssNMR, where the peptide is fully extended within the

fibril core[38] and β-strands adopt a parallel, in-register arrangement.[39] An extension at the C-terminus of the TTR1 sequence produces fibrils that display the hydrophillic bioactive ligands GGRGDS, GGRADS and cycloRGDfK on the fibril surface.[9, 10] Most recently, TTR1-GGE was used to create hybrid nanostructures, where amyloid fibrils were grown within DNA constructs in order to form patterned nanofibrous materials.[40] A new peptide TTR1-GGK was also employed in the later study to tether the fibrils inside the origami sheath. This expanding family of six TTR1 peptides provides an interesting model for fibril assembly, as each peptide shares a common core structure, yet single amino acid differences in the non-core sequences have been shown to impact on the assembly process.[15]

In this study, we investigate the assembly of the TTR1-GGK peptide, characterise the fibril structure and compare fibril properties to other TTR1-based functional fibrils. The TTR1-GGK peptide is attractive as a fibril forming peptide for three reasons. Firstly, the lysine residue provides a simple group for functionalisation following fibril formation. Secondly, the addition of the hydrophilic lysine residue is expected to improve the assembly process, potentially avoiding the irregular assembly of the TTR1 parent peptide[15] where fibrils have varied morphology and form a gel. Finally, the TTR1-GGK peptide has a positive charge, the magnitude of which changes as a function of pH, allowing the effect of environmental conditions such as salt to be examined during fibril formation. Here, we examine the effect of ionic strength, pH and the presence of anions and cations on the assembly of the TTR1-GGK peptide, to test the suitability of this peptide as a fibrous material and to further our understanding of the effect of peptide sequence and physicochemical factors on the assembly and structure of amyloid fibrils from synthetic peptide sequences.

2.0 Results and Discussion

Properties of the TTR1-GGK peptide

The C-terminus of the TTR1-GGK peptide contains a simple functional sequence consisting of glycine-glycine-lysine, or GGK in single amino acid code, which has been added to the base fibril forming TTR1 sequence (Figure 1a). As the pKa of lysine is ~9.3, this hydrophilic residue will carry a positive charge over a wide range of solution pH. The lysine residue has previously been used to create a cationic peptide amphiphile molecule to form β-sheet rich nanofibres.[41] The hydrophilic three residue addition to TTR1 here is expected to alter the

kinetics of fibril assembly, similar to the bioactive functional groups GGRGDS (TTR1-RGD peptide) or GGRADS (TTR1-RAD peptide),[15] improving the ease of peptide handling compared to the parent TTR1 sequence.

The TTR1-GGK peptide is well suited to study electrostatic interactions and fibril formation. The peptide is predicted to have an isoelectric point (pI) of 8.5[42] and a net positive charge of 1.93 at pH 2.0, the conditions typically used for the assembly of TTR1-based fibrils.[10, 15, 43] The net positive charge arises from the N-terminus, C-terminus and two ionisable amino acids, lysine and tyrosine. Like the TTR1-RGD and TTR1-RAD peptides, TTR1-GGK is expected to have a random coil structure when initially dissolved in an aqueous solution, making it a simpler system to explore compared to globular proteins, where the native structure must first be destabilised.

The lysine residue in TTR1-GGK provides an amino group at a location where the peptide is expected to be excluded from the fibril core and available for later chemical coupling. This residue is better suited to functionalisation than the arginine present in TTR1-RGD or TTR1-RAD, due to improved accessibility at the peptide C-terminus and the lower pKa (9.3 c.f. 12), offering improved efficiency for derivatisation closer to neutral pH.[44] The higher pI of TTR1-GGK (8.5 c.f. 5.52-5.83 for TTR1-RGD or TTR1-RAD) and improved solubility near neutral pH also raises the possibility of producing TTR1-GGK fibrils at physiological pH that could be later co-functionalised with pH sensitive groups such as oligonucleotides.[40] These properties are expected to make TTR1-GGK a better unfunctionalised TTR1-based sequence for future studies compared to the parent TTR1 sequence.

Intrinsic peptide properties important for aggregation

Key parameters that will affect the aggregation of the TTR1-GGK peptide include sequence β-sheet propensity, hydrophobicity, net charge and aggregation propensity. The TTR1-GGK peptide has a high β-sheet propensity when assessed using the Street and Mayo scale (Figure 1b).[45] The peptide contains a hydrophobic base sequence (residues 3-7, Figure 1c) due to the inclusion of the TTR1 sequence and this section is expected to play a central role in fibril formation.[46] These residues also display a high aggregation propensity, as predicted by the Waltz (residues 1-8),[47] TANGO (residues 2-7),[48] Aggrescan (residues 1-8)[49] and the Zyggregator algorithms (residues 1-5).[50] These algorithms consistently predict the

hydrophobic peptide sequence as central to peptide aggregation, as occurs for other TTR1-based peptides.

Residues 9 – 14 containing the additional GGK sequence do not contribute to any predicted aggregation propensity using the same algorithms, although these residues have some β-sheet propensity (Figure 1b). Consequently the hydrophilic sequence GGK is expected to be excluded from the fibril core and solvent accessible. The lysine residue is the most hydrophilic of all 14 residues within the peptide sequence (Figure 1c) and the addition of the GGK residues clearly changes the chemical properties of the C-terminal end of the TTR1 peptide.

Assembled TTR1-GGK fibrils have a cross-β core

Fibrils were initially assembled from the TTR1-GGK peptide in a solution of 10% (v/v) acetonitrile (CH_3CN) and 90% (v/v) Milli-Q water at pH 2.0, conditions typical for TTR1-based fibril assembly.[10, 43] Peptide conversion to fibrils was rapid; 63% of the TTR1-GGK peptide had converted to fibrils after 7 days and 79% after 28 days. Fibrils aged for 28 days were considered mature and used for all further characterisation experiments.

Samples of dried TTR1-GGK fibrils were examined by X-ray fibre diffraction to determine the core fibril structure. The wide angle X-ray scattering (WAXS) patterns obtained were characteristic of a cross-β core structure (Figure 2a). The anisotropic reflections observed correspond to a spacing of 4.7 Å and 9.0 Å, arising from the distance between β-strands and between β-sheets respectively (Figure 2b). A further reflection observed at 3.8 Å, is common to other TTR1-based fibrils and may correspond to the Cα–Cα separation distance in polypeptide chains.[51]

The small angle X-ray scattering pattern (SAXS, Figure 2c) obtained from the same fibril samples displayed an anisotropic reflection in the equatorial direction at ~46 Å (Figure 2d), which is likely the width of a single β-sheet within these fibrils. This reflection indicates that most of the TTR1-GGK residues are incorporated into the β-strand, as the full length of the peptide is predicted to extend to ~47 ± 2 Å (based on the average amino acid length in the TTR1 peptide, which when fully extended is 37 ± 2 Å).[38] The error associated with these measurements, however, allows for the possibility that the terminal lysine residue in each

TTR1-GGK peptide may be exposed from the fibril core. A similar reflection is seen for other TTR1-based peptides, which show equatorial reflections in order of extended peptide length; TTR1-RGD and TTR1-RAD fibrils generate a reflection at 52 ± 2 Å (both 17 residue peptides) and TTR1 fibrils a reflection at 36 ± 3 Å (an 11 residue peptide).[10] These X-ray diffraction data indicate that the size of the individual subunits within TTR1-based fibrils is determined by the length of the peptide sequence, although it remains difficult to determine the exact number of residues exposed on the outside of the fibril via this technique.

A series of complementary fibre diffraction experiments were performed to further probe the structure of the TTR1-GGK fibrils. WAXS patterns were obtained from fibrils assembled from the TTR1-GGK peptide in the presence of fragmented mature TTR1-GGK fibrils, in a process known as seeding. The position of the reflections in the pattern obtained for seeded TTR1-GGK fibrils at 4.7 Å and 9.0 Å were similar to these obtained for unseeded samples (Figure 2e). This was expected, since the seed was produced from fibrils assembled from the same TTR1-GGK sequence. The diffraction pattern for seeded fibrils (SI Figure 1a) showed a higher degree of order, consistent with observations made for seeded fibrils of other seeded TTR1-based fibrils.[15]

WAXS patterns obtained from a hydrated pellet of unseeded fibrils displayed reflections at ~4.7 Å and ~9.1 Å, in a similar position to the pattern from dried samples, showing that the cross-β core structure is resistant to dehydration (Figure 2f). The reflections were not detectibly anisotropic due to a low signal to noise ratio (SI Figure 1b) but this is often typical for a hydrated sample, since X-ray scatter due to water is broad and can coincide with the area of interest in the diffraction pattern.

The accessibility of the amine groups at the N-terminus and on the lysine residue in the TTR1-GGK peptide and fibrils was measured using a fluorescamine probe that increases in fluorescence intensity upon binding to primary amines.[52] When free in solution the TTR1-GGK peptide shows greater fluorescence intensity than the TTR1 peptide due to the presence of the lysine residue (Figure 2g). The non-linear increase in fluorescence between TTR1 and TTR1-GGK suggests the flurophore experiences a different chemical environment at the peptide N-terminus compared to the lysine residue.[52] Peptide conversion is similar for both fibril systems,[10] so the fluorescence intensity decrease for both TTR1-GGK and TTR1 after fibril formation suggests some primary amines are now solvent inaccessible within the fibril

core or between protofilament units.[52] The later explanation is more consistent with SAXS observations (Figure 2c,d). Similar observations of the exposure of non-core residues have now been made for several fibril forming systems using a variety of techniques.[53, 54] The high fluorescence observed for TTR1-GGK fibrils compared to TTR1 fibrils indicates that a high proportion of the lysine residues are accessible. This has implications for fibril formation in this study, as lysine will interact with salt ions, it also suggests these lysine residues are accessible for later functionalisation.

The schematic diagram in Figure 2h displays the possible arrangement of peptides within the TTR1-GGK fibril. The β-strand includes the two glycine residues with the lysine residue excluded from the fibril core. This arrangement is based on the position of SAXS reflections and fluorescamine binding to TTR1-GGK fibrils. The lack of a small angle reflection at ~9.1 Å (2 × 4.7 Å) suggests a parallel arrangement of the β-sheets within the fibril core, consistent with other TTR1-based fibrils.[9, 38, 39] These results further highlight the robust nature of TTR1 assembly and show that this peptide sequence is particularly suited for material applications, where a consistent fibril core with known properties may be desirable.

The morphology of TTR1-GGK fibrils in a dried or cryo-preserved state was examined next by Transmission electron microscopy (Figure 3a,b). In both cases the fibrils observed had a regular appearance with a high persistence length (>1 μm) and a ribbon-like morphology. Typically fibrils were 21 ± 2 nm in width (n = 100, mean ± SD) and were regularly twisted with a periodicity of 125 ± 9 nm (n = 100, mean ± SD).

The appearance of these fibrils is more similar to TTR1-RGD and TTR1-RAD fibrils than fibrils assembled from the TTR1 base sequence.[10] The relative order of fibril widths measured using microscopy images is TTR1-RGD ~ TTR1-RAD > TTR1-GGK > TTR1. This order corresponds with the predicted length of extended β-strand[38] and observed length determined by SAXS. The regularity of TTR1-GGK fibril morphology suggests an additional charge at the carboxyl-terminus has influenced protofibril packing, as these fibrils are more regular than those typically assembled from the parent TTR1 peptide. The high persistence length seen for all fibrils (Figure 3) is also an indication of fibril strength[55] and suggests the rates of fibril breakage for the mature fibrils may be low.

The role of lysine in TTR1-GGK fibril formation

The effect of the addition of the residues GGK on the kinetics of fibril formation was assessed for seeded and unseeded samples. Seed fibrils were formed from mature TTR1-GGK fibrils by repeated freeze-thawing (Figure 4a). This treatment readily reduced the length of the fibrils to 68 ± 40 nm (n = 100, mean ± SD) generating two different morphologies; some seeds resembled the mature fibril and retained their twisted appearance, while others appeared shorter and somewhat flatter.

The kinetics of fibril formation was monitored by measuring the solution absorbance at 330 nm as a function of time. A sigmoidal function was fitted to the growth curve to determine the kinetic parameters and to allow simple comparisons between the rates of fibril assembly under different solution conditions. In the absence of seed fibrils, the assembly of TTR1-GGK peptide in 10% (v/v) CH_3CN produced a growth curve with a lag time (t_l) of ~17 h and exponential growth phase of ~0.7 h^{-1} (Figure 4b), characteristic of the nucleated formation pathway seen for amyloid fibril formation.[1] The slight incline in the unseeded turbidity measurement during the lag time may be due to primary nucleation, which is considered a slow process.[56] The addition of seed fibrils at 5% (v/v) to solutions of the TTR1-GGK peptide produced a curve with no observable lag time (Figure 4b) providing further evidence that the formation of TTR1-GGK fibrils is via a nucleated pathway.

The change in turbidity observed for seeded and unseeded preparations of TTR1-GGK peptide corresponded well to changes in the hydrodynamic radius (D_h) observed by dynamic light scattering (DLS) (Figure 4c). The TTR1-GGK peptide displayed a D_h of 3 ± 1 nm. This measurement is less than the predicted size of ~4.7 nm for the extended length of the TTR1-GGK peptide, based on the TTR1 sequence[57] and indicates that the peptide is monomeric when freshly dissolved in a solution of 10% (v/v) CH_3CN, potentially in a more compact form than in TTR1-GGK fibrils. Fragmented fibril seeds displayed a D_h of 71 ± 7 nm, similar to measurements obtained from microscopy images of 68 ± 40 nm (Figure 4a) and comparable to the size of seed fibrils derived from other TTR1-based fibrils.[15] Samples of seeded and unseeded fibrils measured at the end of the growth phase (as assessed by turbidity) contained significantly larger species with a D_h of 1359 ± 55 nm and 1930 ± 358 nm respectively.

The length of the lag time in TTR1-GGK fibril assembly, t_l, was ~17 h for unseeded fibrils and ~0.2 h for seeded fibrils (Figure 4d). The seed fibrils were highly efficient at nucleating fibril growth (Figure 4e) and resulted in a growth curve with an elongation rate constant (k) that was ~6 times faster than observed for unseeded fibril growth. The length of the lag time was inversely proportional to the elongation rate for unseeded and seeded formation, as observed previously for other fibril systems.[58]

Interestingly, the TTR1-GGK peptide displayed a different assembly pathway compared to other TTR1-based peptides, despite the similarity of the core sequence (residues 1 – 11) and charge profile. The lag time for TTR1-GGK is ~3 – 8 times slower than for TTR1-RAD and TTR1-RGD peptides respectively and the rate of elongation for TTR1-GGK is ~2 – 4 times slower respectively. These results indicate that the aggregation propensity of TTR1-GGK is reduced compared to these other modified peptides. The Zyggregator algorithm predicts the relative order of aggregation propensity as TTR1-RGD (0.78) > TTR1-RAD (0.81) > TTR1-GGK (1.05),[50] which follows the experimental order determined here. This order also follows the order predicted by the Wimley-White hydrophobicity scale, which is a measure of the free energy change when a protein moves from water to a bilayer interface. By this scale the peptides are ranked; TTR1-RGD (+14.53 Kcal.mol^{-1}) > TTR1-RAD (+13.88 Kcal.mol^{-1}) > TTR1-GGK (+10.27 Kcal.mol^{-1}).[59] These results illustrate the importance of the intrinsic properties of the peptide sequence, including any hydrophilic extensions, in determining the rates of fibril elongation. This trend occurs despite the phenomenon of fibril breakage in secondary fibril formation.[7, 56] These comparisons also show that while hydrophobic interactions play a key role in TTR1-based fibril assembly, the hydrophilic nature of a fibril forming peptide should also be considered when designing functional fibrils, as these residues can alter fibril formation in polar solvents.

The effect of ionic strength and pH on TTR1-GGK fibril formation

The concentration of salt in a solution is known to alter the propensity of a polypeptide sequence to assemble into fibrils[60] but it is unclear how these conditions effect fibril formation from synthetic TTR1-based sequences. We therefore set out to determine the effect of salt concentration and solution pH on the kinetics of TTR1-GGK fibril formation. The TANGO algorithm predicts an increase in β-sheet aggregation propensity for the TTR1-GGK peptide with increasing ionic strength (Figure 5a). The core residues (residues 2-7) contribute

to this increase in propensity, consistent with the role of these residues in hydrophobic interactions thought to occur during fibril assembly. In contrast, the C-terminal residues of the TTR1-GGK peptide do not contribute to this increase.

The salt sodium chloride (NaCl) was selected for initial experiments to assess the effects of solution ionic strength, as this salt is considered to have the mildest effect of all salts on protein solubility, allowing subtle effects to be examined.[28] A concentration of 50 mM, 100 mM , 250 mM or 500 mM NaCl, was selected, corresponding to the range of ionic strengths expected to influence TTR1-GGK assembly, as indicated by the TANGO algorithm (Figure 5a). Nucleated-growth curves were observed in the presence of NaCl (Figure 5b), similar to the kinetics observed in salt-free conditions using 10% (v/v) CH_3CN (Figure 4b). The growth curves displayed systematic changes with increased ionic strength. Most notable was the decrease in lag time and increase in the final absorbance measured. The possibility of peptide precipitation under these conditions was explored before kinetic comparisons.

Dynamic light scattering measurements were used to measure the hydrodynamic radius, D_h, of freshly dissolved TTR1-GGK peptide in the presence of an increasing concentration of salt. A D_h of 2 – 3 nm was measured for all salt concentrations tested (Figure 5c), similar to the peptide in 10% (v/v) CH_3CN (Figure 4c, 3 ± 1 nm). This similarity in size suggests that these conditions are below the critical concentration for spontaneous precipitation seen for other peptide systems with increasing ionic strength.[24] The observed increase in final absorbance at the end of kinetic measurements (Figure 5b) is therefore unlikely to be a result of peptide precipitation.

The lag time t_l determined from the kinetics of TTR1-GGK assembly in the presence of salt was systematically reduced with the increase in solution ionic strength (Figure 5d, Table 1), from t_l ~17 h in salt-free conditions to t_l ~2 h in a solution with an ionic strength of 500 mM (500 mM NaCl, Table 1, $p < 0.01$). This increase in nucleation propensity correlates well with TANGO predictions (Figure 5a) and is consistent with the expected reduction in the repulsive interactions between peptides.[28] Other polypeptide sequences have displayed a similar decrease in lag time with increased ionic strength due to NaCl addition, including: Aβ(1-40), β2-Microglobulin, insulin, the mouse prion protein, α-synuclein, amylin and the α-spectrin SH3 mutant.[24-26, 31, 32, 36, 61] The magnitude of the reduction in lag for TTR1-GGK with a 500 mM increase in ionic strength from no salt to 500 mM NaCl was similar to other

systems. For example, the TTR1-GGK peptide nucleated ~8 times faster while the polypeptides Aβ(1-40)[24] and α-synuclein[32] nucleated ~20 times and ~6 times faster, respectively, in the presence of NaCl.

The elongation rate of TTR1-GGK fibrils was significantly reduced in the presence of increasing concentrations of NaCl, indicating that the addition of peptides to the growing end of fibrils was systematically slower (Figure 5e). This was despite the high nucleation efficiency in the presence of salt (Figure 5d). Interestingly, the elongation rate was fastest with 50 mM NaCl, suggesting that low salt concentrations are optimal for elongation.

The absorbance reached at the end of the kinetic measurements was significantly higher ($p < 0.05$) in the presence of higher concentrations of NaCl (Figure 5f). A similar trend was observed for fibrils formed from glucagon at alkaline pH; where the apparent elongation rate decreased and the final ThT fluorescence intensity increased with increasing ionic strength.[30] The results presented here are in contrast, however, to studies that show a correlation between a reduction in the nucleation time and an increase in the elongation rate for α-synuclein, insulin, Aβ(1-40) and glucagon at acidic pH,[24, 26, 30, 32] suggesting that NaCl interacts differently with the peptide that is being added to the end of the elongating fibril in both these systems.

The effect of divalent cations and solution pH on TTR1-GGK fibril formation

The effect of a second salt, calcium chloride ($CaCl_2$), on the assembly of TTR1-GGK fibrils was examined next using an extended range of solution pH: pH 2.0, pH 6.5 and pH 10.5. The $CaCl_2$ salt provides an interesting comparison to NaCl since the divalent cation Ca^{2+} can be used to explore the possibility of ionic bridge formation, a type of bonding that is sensitive to changes in pH.[28] Ionic bridges may occur between the peptide carboxyl terminus and the Ca^{2+} ion at alkaline pH when the carboxyl terminus is ionised. Such preferential specific binding sites can also alter significantly the interactions between ions and proteins.[62] The pH range selected here spans the theoretical pI (8.5) for the peptide allowing the effect of peptide charge to be explored. The peptide has a net charge of +1.93 at pH 2.0, +0.97 at pH 6.5, and -2.35 at pH 10.5.

The TANGO algorithm predicts the TTR1-GGK peptide will have a high β-aggregation propensity in 50 mM $CaCl_2$, with subtly altered aggregation propensity as a function of solution pH (Figure 6a), reflecting the change in peptide net charge and possible electrostatic interactions. It is also expected that the TTR1-GGK peptide will aggregate more readily in the presence of 50 mM $CaCl_2$ salt at pH 2.0 (β-aggregation of ~58, ionic strength 130 mM) compared to a solution of 50 mM NaCl at pH 2.0 (β-aggregation of ~49, ionic strength 50 mM) or 10% (v/v) CH_3CN (β-aggregation of ~35, ionic strength 0 mM).

Experimentally, TTR1-GGK fibril assembly was promoted by the addition of $CaCl_2$ at each pH tested (Figure 6b and c). The length of the lag time, t_l, was significantly reduced in 50 mM $CaCl_2$ at pH 2.0 (t_l of 4.1 ± 1 h) compared to assembly in 50 mM NaCl at pH 2 (t_l 10 ± 1.2 h) or 10% (v/v) CH_3CN at pH 2 (t_l of 16.8 ± 3.1 h). This decrease in the duration of the lag time for TTR1-GGK fibril formation is consistent with TANGO predictions (Figure 6a), indicating that a reduction in electrostatic repulsion by screening the net positive charge on the TTR1-GGK peptide is responsible for a decrease in the lag time observed.

At a constant salt concentration (50 mM), $CaCl_2$ has a higher ionic strength than NaCl. When the lag time for TTR1-GGK fibril assembly is compared at constant salt concentration, $CaCl_2$ (ionic strength 130 mM, t_l of 4.1 ± 1 h) induces a shorter lag time than NaCl (ionic strength 50 mM, t_l 10 ± 1.2 h), as expected for electrostatic screening effects. When the lag time is compared on the basis of equal Cl^- concentration, that is a salt concentration of 50 mM $CaCl_2$ (t_l of 4.1 ± 1.0 h) or 100 mM NaCl (t_l of 4.9 ± 1.7 h), the lag times were similar, consistent with electrostatic repulsion effects dominating TTR1-GGK fibril nucleation.

If electrostatic effects alone were responsible for TTR1-GGK fibril nucleation then it would be expected that at higher ionic strengths the lag time should decrease regardless of the cation type. The lag times in 50 mM $CaCl_2$ (ionic strength 130 mM) and 250 mM NaCl (ionic strength 250 mM) however, are similar ($CaCl_2$ t_l of 4.1 ± 1.0 h and NaCl t_l of 4.0 ± 1.5 h). This observation indicates that an increase in ionic strength alone is not solely responsible for TTR1-GGK peptide nucleation at least at higher ionic strengths, within the range expected for ion specific effects (~100 mM).[28] A similar approach was taken to determine cation-specific effect on the duration of the lag time for β-lactoglobulin fibril formation.[35]

The lag times (t_l) observed at the two extremes of pH at 2.0 and 10.5 at 50 mM $CaCl_2$ were ~1.7 fold slower than at the intermediate pH of 6.5 ($p < 0.05$), indicating that a balance of electrostatic and hydrophobic interactions is important for initial inter-peptide contacts, as the TTR1-GGK peptide carries the lowest net charge of +0.97 at pH 6.5 (c.f. +1.93 at pH 2.0 and -2.35 at pH 10.5).[63, 64] The similarity in the lag time at pH 2 and pH 10.5 is also an indication that ionic bridges are not promoting the approach of TTR1-GGK peptides. The *k* values, representing the rate of fibril elongation were similar at pH 2.0 and pH 6.5 and slightly reduced at pH 10.5 (Figure 6c). These rates were not significantly different to those observed for assembly in 10% (v/v) CH_3CN alone (k 0.7 ± 0.3 h^{-1}) or NaCl at 50 mM pH 2.0 (k 1.46 ± 0.12 h^{-1}). There was no obvious correlation between the lag time t_l and the rate of elongation *k* for the data obtained from these experiments (data not shown).

Effect of various salts on TTR1-GGK fibril assembly

A range of different monovalent and divalent salts in were selected to further explore any ion specific effects[28, 29, 62, 65] on the assembly of the TTR1-GGK peptide into fibrils using a salt concentration of 50 mM, similar to experiments with the salts NaCl and $CaCl_2$ (Figures 5 and 6).

The monovalent anions tested were sodium chloride, sodium iodide and sodium nitrate (NaCl, NaI, and $NaNO_3$, Table 1). These salts explore the effect of different anions on TTR1-GGK fibril assembly by keeping the counter-ion (Na^+) constant. The total ionic strength is also constant at 50 mM and may be used to see any anion specific effects. All sodium (Na^+) paired monovalent anions Cl^-, I^- and NO_3^- significantly ($p < 0.05$) decreased the lag time, t_l, of TTR1-GGK assembly compared to 10% (v/v) CH_3CN (Figure 7a). This observation is consistent with peptide charge screening effects seen for earlier experiments (Figures 5d and 6b). Relative to the I^- and NO_3^- anions, Cl^- was the least effective at promoting nucleation for TTR1-GGK, as previously observed for β_2-Microglobulin, glucagon and the mouse prion protein.[25, 30, 31] The order of monovalent anions is also consistent with the order of the strength of the chaotrope ($I^->NO_3^->Cl^-$), indicating anion-specific effects are acting on the TTR1-GGK peptide in solution, promoting peptide hydration and the approach of hydrophobic core residues.[28, 29] The elongation rate, *k*, was generally faster with added salt (Figure 7b) compared to 10% (v/v) CH_3CN. The exception was $NaNO_3$. No significant differences were seen between the final absorbance measurements for these experiments.

Next, the monovalent cations sodium chloride, lithium chloride and potassium chloride (NaCl, LiCl and KCl, Table 1) were tested. For this salt series the chloride counter-ion was kept constant, allowing the effect of different cations on TTR1-GGK fibril assembly to be explored. The total ionic strength was also constant (50 mM). All chloride (Cl^-) paired salts examined significantly ($p < 0.05$) reduced the lag time t_l compared to assembly in 10% (v/v) CH_3CN (Figure 7c). This is consistent with charge screening effects observed previously (Figure 5d, Figure 6b and Figure 7a). The salt LiCl was most efficient at nucleating fibril formation. The lag time, tl, observed in the presence of the other salts were in the relative order $Li^+ > K^+ > Na^+$. The elongation rate, *k,* was faster in the presence of various cations tested, compared to 10% (v/v) CH_3CN (Figure 7d), in good agreement with observations made for the anions. Again, no significant differences were seen between the final absorbance measurements for these experiments and no other systematic trends observed.

The effect of divalent cations on TTR1-GGK fibril assembly was next examined using calcium chloride and magnesium chloride ($CaCl_2$, $MgCl_2$), the divalent anion sodium sulphate (Na_2SO_4) was also included in this comparison. The total ionic strength was kept constant at 130 mM. The divalent cations (Ca^{2+} and Mg^{2+}) and anion (SO_4^{2-}) examined significantly ($p < 0.05$) reduced the lag time, t_l, compared to assembly in 10% (v/v) CH_3CN, as expected (Figure 7e). The elongation rate was not significantly different using divalent cations compared to no salt (Figure 7f), which is different to the monovalent cations, which induced a faster rate of elongation (Figure 7c). The addition of the divalent anion, however, did increase the rate of fibril elongation (Figure 7f). No significant differences were seen between the final absorbance measurements for the divalent ions tested.

The order of the effect of the monovalent anions $I^- > NO_3^- > Cl^-$ observed is in good agreement with the order of the strength of chaotropes (from strongest to weakest chaotrope $I^- > NO_3^- > Cl^-$ respectively).[28] Chaotropes increase protein solubility by promoting the hydration of the protein in solution, leading to the exposure of more protein surfaces to the solvent[28] and consequently fibril formation. The addition of the monovalent anions likely screens repulsion between peptides, while specific ion effects promote the solubility of the peptide in solution, allowing for the approach of hydrophobic sections of the protein.

To further understand the role of ion hydration on the lag time, t_l, for TTR1-GGK fibril formation the data describing the effect of monovalent chaotropic anions (I^-, NO_3^- and Cl^-) was compared to the data obtained for the divalent kosmotropic anion (SO_4^{2-}). The lag time was similar in the presence of Na_2SO_4 (*tl* of 2.9 ± 0.6 h, ionic strength 130 mM), NaI (*tl* of 2.4 ± 0.1 h, ionic strength 50 mM) and $NaNO_3$ (*tl* of 2.7 ± 0.1 h, ionic strength 50 mM), despite the total ionic strength being ~2.6 times higher in the solution with Na_2SO_4. In contrast, the lag time in NaCl (*tl* of 10 ± 1.2 h, ionic strength 50 mM) was longer than in the presence of Na_2SO_4, reflecting the weak chaotropic nature of the NaCl salt. These results indicate that chaotropic salts have a stronger effect on fibril nucleation that is independent of the solution ionic strength.

In addition to electrostatic repulsion and ion interactions at the protein-water interface, direct anion binding may also affect the lag time for TTR1-GGK fibril formation. Positive charges are expected to be present on the TTR1-GGK peptide at the N-terminus (+0.93) or on the lysine side chain (+1) at pH 2, creating the conditions for anion binding. The strength of direct anion binding is typically described by the electroselectivity series, where the relative order of anions is $SO_4^{2-}>I^->NO_3^->Cl^-$.[66] The lag time for TTR1-GGK aggregation followed the relative order $I^->NO_3^->Cl^-$expected in this series (Table 1), although the lag time for SO_4^{2-} ion was not significantly faster in the presence of these anions, as would be expected if direct anion binding played a large role. This result indicates that the chaotropic effect of anions is more important than direct anion binding in fibril formation. The selection and testing of a wider range of kosmotropic anions may decouple some of these effects with greater certainty.

The effect of the cations on TTR1-GGK assembly was next compared. The effect of K^+ was stronger than Na^+, consistent with the most chaotropic ion promoting fibril formation[28] and as seen for the anions. The ion Li^+ had the strongest effect of the three monovalent cations examined, however, despite it being a kosmotropic ion, indicating that cations may act differently to the anions. From these results it is difficult to determine a trend from the monovalent cations tested and the selection and testing of a wider range of chaotropic cations may decouple some of these effects.

The effect of all the cations tested on TTR1-GGK nucleation, including the monovalent and divalent cations, can be ranked as $Ca^{2+}>Mg^{2+}>Li^+>K^+>Na^+$. This order is effectively the reverse order of the Hofmeister series $K^+>Na^+>Li^+>Mg^{2+}>Ca^{2+}$.[28] A similar reverse order

was observed for the Aβ(1-40) peptide with Mg^{2+}>Li^{+}>Na^{+}>K^{+}.[24] The reverse order may be due to the nature of the TTR1-GGK peptide, in which the residues 3-7 (Figure 5.2b) are hydrophobic and a net positive charge of +1.93 (Figure 5.1b) arises from the N-terminus (+0.93) and the lysine side chain (+1). These peptide properties may account for the reverse order seen, as ions are known to interact with a hydrophobic surface and positive surface charges.[28] This result is also consistent with the reverse order of the Hofmeister series seen the α-synuclein fibril formation, when the peptide was examined at a pH below the pI (i.e. when the peptide had a net positive charge).[32]

The effect of salt on TTR1-GGK fibril morphology and structure

The changes in the kinetics of TTR1-GGK assembly seen with the addition of various salt ions, increasing salt concentration and change in pH prompted an examination of fibril morphology and structure. Ribbon-like fibrils with an elongated morphology were observed by TEM for all solution conditions tested (SI Figure 2), confirming that TTR1-GGK fibrils had similar appearance despite the altered kinetics of assembly. Qualitatively similar numbers of fibrils were seen at each condition. At higher concentrations of salt, TEM images show some indication of fibril untwisting (SI Figure 2). The size of the periodic pitch for each fibril was measured (SI Figure 6) in each of the different solution conditions, although no significant differences in pitch were observed (SI Table 3). TEM may not be the most ideal technique to measure the length of the twist length, as salt may be concentrated when samples are dehydrated during preparation and hydrated techniques such as atomic force microscopy may be more suited to determining changes in pitch.[37, 67] The TTR1-GGK fibrils remained long and did not appear shortened at salt concentrations up to 250 mM (in NaCl).

The secondary structure of TTR1-GGK peptide in the presence of salt was examined using circular dichroism (Far-UV CD). The TTR1-GGK peptide adopts a random coil structure (Figure 8a) for all conditions examined.[68] Data from wavenumbers less than 200 nm were excluded from analysis due to the scattering induced by the salt ions. The unordered structure indicates the salts and solution conditions do not change the initial peptide structure prior to fibril formation. A similar observation was made for another unstructured peptide Aβ(1-40).[24] The CD data confirm that the differences seen in the kinetics of fibrils TTR1-GGK assembly (Figures 5 – 7) are not confounded by differences in intrinsic peptide structure.

The secondary structure of mature TTR1-GGK fibrils was also examined using far-UV CD. The peptide adopts a β-sheet secondary structure consistent with fibril formation, as shown by the decrease in mean residue ellipiticity ([Θ]) at 217 nm (Figure 8b). The magnitude of the decrease in [Θ] is similar to that observed for fibrils assembled in 10% (v/v) CH_3CN, $CaCl_2$ or low concentrations of NaCl (Figure 8c). This difference between [Θ] at 217 nm for peptide and fibrils was less marked with higher concentrations of NaCl, possible reflecting noise in these spectra.

Attenuated total reflectance – Fourier transform infrared (ATR-FTIR) spectroscopy also confirms a β-sheet secondary structure within TTR1-GGK fibrils (Figure 8d). All spectra contain an amide I peak that corresponds to C=O stretching at 1628-1630 cm^{-1} and a minor peak at 1670 – 1672 cm^{-1}that indicates β-sheet secondary structure, consistent with the spectra for TTR1 and TTR1 functionalised fibrils, which contain maxima at 1628 – 1629 cm^{-1} [3, 9] (see supplementary information SI Table 1 for the amide I peak position for each condition). No peak is observed at ~1684 cm^{-1}, consistent with the predicted parallel arrangement of the fibril core (Figure 2). In the amide II region, peaks arising from N-H bending and CN stretching observed at 1543 – 1547 cm^{-1} and 1517 – 1518 cm^{-1} were consistent between samples.

While some variation is observed between the FTIR spectra for fibrils assembled in different conditions, this variation is small. The amide I peaks in the spectra for fibrils assembled in $CaCl_2$ with different pH were broader (Figure 8e). This is less apparent, however, when IR spectra were collected for fibrils assembled under the same conditions in D_2O and examined in transmission mode (Figure 8f), where the spectra for fibrils in 10% (v/v) CH_3CN were broader. At least 94% of peptide was converted to fibrils after 7 days in 50 mM $CaCl_2$ at pH 2.0, increasing to 95% after 28 days. This confirms any differences are likely the result of subtle structural changes in mature fibrils.

X-ray diffraction patterns indicate that the core structure within the fibrils formed by TTR1-GGK under different solution conditions is highly similar. Reflections were observed at ~4.7 Å and ~9.0 Å for all treatments (X-ray patterns are given in SI Figure 3, X-ray profiles in SI Figure 4 and the position of reflections in SI Table 2). A hydrated WAXS profile was obtained for TTR1-GGK fibrils assembled in $CaCl_2$ (SI Figure 5), since the FTIR spectra differed for fibrils assembled in a solution of Ca^{2+} or 10% (v/v) CN_3CN but were similar for

fibrils assembled in $CaCl_2$ or 10% (v/v) CN_3CN in D_2O. The reflections observed at ~4.7 Å and ~9.0 Å (SI Table 2) confirmed a cross-β core in these fibrils, illustrating that the presence of $CaCl_2$ had only a subtle effect on the fibril secondary structure and not on the arrangement of the fibril core.

Together, the morphological, secondary structure and X-ray diffraction data for TTR1-GGK fibrils assembled in the presence of a range of salts suggest that while the salts examined alter the kinetics of fibril assembly, they have only a subtle effect on fibril secondary structure and do not significantly alter fibril appearance or the fibril core structure, which is known to impart many fibril properties [69].

3. Conclusion

This study characterised fibrils formed by the TTR1-GGK peptide. This peptide is better suited for biomaterials applications than the parent TTR1 peptide, as the GGK residues improve peptide handling and provide an amine group that is solvent accessible on the surface of fibrils ready for functionalisation. This modification potentially allows both ends of the peptide to be modified simultaneously following fibril formation via the amine at the N-terminus and side chain of the lysine residue at the C-terminus. TTR1-GGK fibrils have a uniform morphology and the core structure common to other TTR1-based fibrils. Comparisons to TTR1-RGD and TTR1-RAD fibrils illustrate the importance of C-terminal peptide extensions in determining the length of the β-strand within the fibril core, the width of mature fibrils and the relative rates of fibril assembly.

The duration of the lag time for TTR1-GGK peptide fibril formation was systematically reduced with increasing ionic strengths from 0 mM to 500 mM using NaCl. This result indicates that electrostatic repulsion between TTR1-GGK peptides in solution is a major factor in the length of the nucleation time, with specific ions strongly affecting the lag time. The behaviour induced by anions could be ordered by their chaotropic strength, while the behaviour induced by cations generally followed the reverse Hofmeister order. These results indicate that salts play a complex role in TTR1-GGK fibril formation; the nucleation of theTTR1-GGK peptide is strongly affected by peptide-peptide repulsion and the solubility of the hydrophobic region of the peptide. The interactions observed in the presence of anions here suggest that the hydrophobic association required to form fibrils could be promoted by

the addition of strong anionic chaotropes, which act on proteins by increasing their solubility. Further studies that alter the ionic strength of the salts tested here may provide greater insights into the effect of cations.

The data presented in this study provide evidence that while the effect of salts on some fibril forming systems can be described by either the electroselectivity series or Hofmeister series, interactions with other polypeptides such as the synthetic TTR1-GGK peptide are more complex. Our study provides insights relevant to the aggregation processes occurring in disease and has implications for industrial processes involving protein and salt and the storage of therapeutic peptides. Our findings also show the robust nature of TTR1 directed assembly. They illustrate that while the rates of nucleation and elongation can be altered by the addition of salt, the characterisation techniques applied here (TEM, FTIR and X-ray diffraction) suggest there are no concurrent changes to the core fibril structure at the length scales examined. While the fibril length and pitch appeared unchanged, changes in fibril morphology, such as partial unwinding, may be visible via other techniques. This work shows that the conditions used for TTR1-based fibril assembly may be altered to suit the requirements of functional molecules that are sensitive to solution pH or ionic strength.

4. Experimental Section

4.1 Peptide synthesis

The peptide TTR1-GGK (YTIAALLSPYSGGK) and the peptide TTR1 (YTIAALLSPYS) were synthesised by CS Bio Company (Menlo Park, CA, USA) and purified by High Performance Liquid Chromatography to >95% purity. The peptide mass was confirmed by Mass Spectrometry (1140 Da and 1198 Da respectively).

4.2 Fibril formation

All solutions were prepared in high purity Milli-Q water of resistivity 18 MΩcm. These were 10% (v/v) CH_3CN, 0.1 M $CaCl_2$ or 1 M stock solutions of $MgCl_2$, LiCl, NaCl, KCl, Na_2SO_4, $NaNO_3$ or NaI. All stock solutions were filtered using a 0.22 μm syringe filter (Millipore, Billerica, MA, USA) and diluted in Milli-Q water to the required concentration prior to use. Peptides were resuspended in the relevant solution at a concentration of 5 mg/ml (unless

712 otherwise indicated). The pH was adjusted where necessary with 1 M NaOH or 1 M HCl
713 using an Orion Micro pH electrode (Thermo Electron Corporation) and the peptide solution
714 then incubated at 37 °C for 24 h. For fibril formation in the presence of fibril seeds, fibrils
715 matured at room temperature for 28 days were fragmented by a freeze-thaw process in liquid
716 nitrogen that was repeated three times. An aliquot of freshly fragmented fibril seeds was
717 added to freshly dissolved peptide at a final seed concentration of 5% (v/v). TTR1 fibrils
718 were assembled in 10% (v/v) CH_3CN as described previously [15], and incubated at 37 °C for
719 24 hours.
720
721 Fibrils matured for 28 days were used for all biophysical characterisation. The efficiency of
722 TTR1-GGK peptide conversion to fibrils at 28 days was assessed for samples assembled in
723 10% (v/v) CH_3CN or 50 mM $CaCl_2$. Fibrils were separated from any remaining free peptide
724 by centrifuging samples at 313,000 g and 4 °C for 50 min in a Beckman XL-1 ultracentrifuge
725 (Beckman Coulter, Inc., USA). The amino acid concentration in the supernatant was
726 determined by amino acid analysis using a ninhydrin-based detection technique.
727
728 The free amine groups accessible on TTR1-GGK and TTR1 peptides and fibrils was
729 measured using Fluorescamine (Sigma-Aldrich, Australia). A 5 µL aliquot of freshly
730 dissolved TTR1-GGK or TTR1 peptide or mature fibrils (10 mg/ml) was added145 µL of
731 PBS (pH 7.4) in a black, clear bottomed 96-well plate (Greiner Bio-one, USA). Each sample
732 was tested using 8 replicates. The plate was placed on a shaker and a 50 µL aliquot of a stock
733 solution of 3 mg/ml Fluorescamine in acetone (AR Ajax Finechem, Nuplex Industries,
734 Australia) was added to each well. The plate was agitated for 1 min and the fluorescence
735 emission at 460 nm (bandwidth 40 nm) was measured using a FLUOstar OPTIMA
736 platereader (BMG Labtech, Germany) using an excitation filter set at 400 nm (bandwidth 30
737 nm). Data were normalised to the mean value obtained for TTR1 fibrils.
738
739 4.3 Bioinformatics
740
741 The TTR1-GGK sequence was scored for hydrophobicity using the Kyte and Doolittle scale
742 [70] and β-sheet propensity using the Street and Mayo scale [45] with a theoretical value for
743 glycine [71]. The net charge was calculated as a function of pH using reported pKa values and
744 the Henderson-Hasselbalch equation [72, 73]. The isoelectric point was estimated using
745 ProtParam from the ExPASy Proteomics Server [42].

Predictions of β-aggregation were obtained using the TANGO algorithm at 310.15 K, using the relevant pH and ionic strength [48]. The Zaggregator [50], Aggrescan [49] and WALTZ [47] algorithms were also used to predict β-aggregation.

4.4 Biophysical characterisation

4.4.1 Transmission electron microscopy

Fibrils were prepared for Transmission electron microscopy (TEM) imaging by diluting (1:50) with Milli-Q water and applying a 3 uL aliquot of this solution to a glow-discharged, carbon-coated and Formvar-film layered 300 mesh copper grid (ProSciTech, Australia). The solution was then allowed to adsorb for 1 min. Grids were rinsed twice with Milli-Q water, negatively stained with uranyl acetate (2% w/v) for 10 s and air dried. Micrographs were acquired using a FEI Company Tecnai TF30 transmission electron microscope (FEI Company, Eindhoven, The Netherlands), fitted with a Gatan US1000 2kx2k CCD camera (Gatan, Inc. Pleasenton, Ca, USA) operated at 300 kV at 8 µm defocus. Fibril dimensions were measured using ImageJ software (NIH, Bethesda, MD, USA) and the pixel size was calibrated using the imprinted scale bar.

For cryo-TEM, fibrils were diluted (1:18) with Milli-Q water and a 3 µL aliquot was applied to a glow-discharged Lacey-carbon grid (ProSciTech, Australia). After 1 min the grid was blotted, then immediately plunge-frozen into liquid ethane using a in-house plunging device. For two-dimensional (2D) imaging, cryoEM was performed on the same Tecnai TF30 microscope held at -170 °C and operated at 300 kV. Images were collected at a magnification of 32,000 X using low-dose operation and applying an underfocus of ~12 µm.

4.4.2 X-ray fibre diffraction

Wide angle X-ray scattering (WAXS) and small angle X-ray scattering (SAXS) patterns were collected for a dried stalk of TTR1-GGK fibrils on the Macromolecular Crystallography beamline [74] and the SAXS/WAXS beamline respectively at the Australian Synchrotron. WAXS patterns were acquired with a sample-to-detector distance of 300 mm, a wavelength of 0.95363 Å and sample exposure time of 1 s. SAXS patterns were acquired with a sample-

to-detector distance of 3338.7 mm, a wavelength of 1.0332 Å and sample exposure time of 1s.

Fibril stalks were prepared by air drying a 10 µL solution of TTR1-GGK fibrils between two wax-filled capillary ends, as described previously [9]. A hydrated fibril pellet was prepared using a centrifugal concentrator (Millipore Amicon Ultra 10 kDa cut-off). An aliquot from the pellet was then placed into a quartz capillary with an inner diameter of 0.3 mm and a wall thickness of 1 mm (Hampton Research Co, USA). Fibrils were aligned by centrifuging the capillary at 500*g* for 5 min and WAXS patterns acquired immediately after centrifugation. Background WAXS patterns were collected by filling an equivalent capillary with a solution of 10% (v/v) CH_3CN.

WAXS images were converted to tiff files using the program fit-2d (Hammersley/ESRF) and radially integrated to generate one dimensional scattering patterns using a Matlab coded integration tool in ImageJ. The integration tool was calibrated with a WAXS pattern of high density polyethylene collected using identical conditions. Fibril WAXS patterns were radially integrated in both the equatorial and axial direction using a 30 degree sector in the azimuthal direction on either side of the reflection. The average one dimensional scattering patterns were scaled at 0.15 $Å^{-1}$ as described previously.[75] For the hydrated sample the background scattering profile was subtracted from the fibril profile. All radial intensity profiles were normalised to the value of maximum intensity and plotted against reciprocal space (1/d $Å^{-1}$) and the peaks used to determine the position of reflections. The error in the peak position for each sample was calculated by the difference in position between two equatorial and two axial profiles. The error in the calibrant was determined by the same process and was multiplied by the error in the peak position as an estimate of the overall error. SAXS diffraction patterns were converted to a one dimensional profile using SAXS15 version 3.229 data analysis software and the intensity profile was normalised to the value of maximum intensity.

4.4.3 Attenuated total reflectance Fourier-transform infrared (ATR-FTIR) spectroscopy

FTIR spectra for TTR1-GGK samples were acquired using a FTIR spectrometer (Universal ATR-FTIR, Perkin Elmer, Waltham, MA, USA). A 2 µl aliquot of fibrils was applied to the

diamond surface and allowed to dry forming a thin hydrated film. Spectra were recorded in attenuated total reflectance mode and datacollected between 4000 cm^{-1} to 650 cm^{-1} with a resolution of 4.0 cm^{-1} and 128 scans co-added. Data in the amide I region showed similar absorbance peak intensity and spectra were normalized to the value of maximum absorbance to aid comparison.

4.4.4 Transmission Fourier-transform infrared (FTIR) spectroscopy

TTR1-GGK fibrils were examined on the Infrared (IR) beamline at the Australian Synchrotron using a Fourier transform infrared (FTIR) spectrometer in transmission mode. Spectra were collected with a Brucker Vertex V80 vacuum FTIR spectrometer and Hyperion 2000 IR microscope (Bruker Optics GmbH., Ettlingen, Germany) using the Bruker OPUS version 6.5 software. The microscope and sample were purged with dry air to minimise water vapour contributions in the spectra. All data was collected at ambient conditions with a spectral resolution of 4 cm^{-1} and 128 scans co-added.

FTIR data was collected for fibril samples formed in solution of a 40 mg/ml peptide suspended in 10% (v/v) anhydrous CH_3CN and 90% (v/v) D_2O (Cambridge Isotopes Inc., USA) or 50 mM anhydrous $CaCl_2$ in D_2O and matured for at least 28 days. A 2 μL aliquot of fibrils was placed between CaF_2 windows separated by a ~6 μm spacer. The maximum absorbance measured for each spectrum was between 0.1 – 1.0 absorbance units. Data in the amide I region was normalized to the value of maximum absorbance to aid comparision.

4.4.5 Circular Dichroism Spectroscopy

The TTR1-GGK peptide was dissolved at a final concentration of 0.15 $mg.ml^{-1}$ in a solution of acetonitrile or salt solution and 1 M HCl used to adjust the solution pH to 2.0. CD spectra were then recorded on a JASCO J-815 CD spectropolarimeter (JASCO, Easton, MD, USA) at 25 °C using a 1 mm pathlength cuvette. The data was acquired between 185 – 300 nm at a scan rate of 50 $nm.s^{-1}$ with a step size of 0.1 nm. The spectra are the average of 6 scans.

4.5 Measurement of aggregation kinetics

Solution turbidity was measured over time to observe the kinetics of TTR1-GGK peptide aggregation using a FLUOstar OPTIMA platereader. The plate chamber was heated to 37 °C and set to agitate for 1 min prior to each measurement in an orbital motion with a 6 mm diameter for each orbital sweep. The excitation filter was set to 330 nm (bandwidth of 10 nm) and measurements were recorded every 5 mins until the turbidity was near constant.

For kinetic experiments the TTR1-GGK peptide was suspended at 10 mg/ml 10% (v/v) CH_3CN or 5 mg/ml in the salt solutions described in section 4. Peptide solutions were immediately loaded into the wells of a clear polystyrene 384-well plate (Nunc polystyrene plate, Denmark) then sealed with transparent adhesive plastic film to prevent evaporation (Excel Scientific., Victorville CA, USA).

Sigmoidal curves were fitted to the turbidity data to allow for simple comparisons between each solution condition. Prior to fitting, the signal from buffer was subtracted from the raw data. The equation used to fit the data was;

$$A_{330nm}(t) = A_{330nm(max)}/1\text{-}\exp(-k(t-t_{50})) \quad \text{(Eq. 1)}$$

where A_{330nm} is the measured absorbance (a.u.), t is time (h), $A_{330nmmax}$ is the maximum absorbance reached (a.u.), k is a kinetic rate constant (h^{-1}) and t_{50} is the time when A_{330nm} is equal to one half of the maximum absorbance $A_{330nmmax}$ (h). The lag time (t_l) was calculated from the second derivative of Eq 1. Each fit correlated to an R^2 value of >0.98 and the reported k and t_l values are the average of replicate samples and the error is the standard deviation calculated from replicate samples.

A Malvern high performance particle sizer (HPPS) with a He-Ne laser (633 nm) was used to measure the dynamic light scattering (DLS) properties of freshly dissolved peptide or solutions of preformed fibrils. The laser was set at an angle of 173° and a temperature of 25 ± 0.1 °C maintained. Peptide solutions with a concentration of 10 mg/ml were used for all DLS measurements. Samples were filtered using a centrifugal filter with a pore size of 20 nm prior to use (Whatmann, United Kingdom), the concentration of the peptide before and after filtration was checked at 280 nm. No significant signal was detected using a blank sample with 10% (v/v) CH_3CN or solutions with NaCl.

879 4.6 Statistical analysis
880
881 Kinetic parameters were tested for statistical difference using the student's t test and
882 probability values of $p < 0.05$ were considered significantly different.
883
884 **Acknowledgements**
885
886 The authors wish to acknowledge the Advanced Microscopy Facility at The University of
887 Melbourne for their technical advice and thank the staff from the Macromolecular
888 Crystallography (MX1/MX2), SAXS/WAXS and IR beamlines at the Australian Synchrotron
889 for their support. FC is supported by the Australian Research Council under the Federation
890 Fellowship scheme.
891
892 **References**
893
894 1. C. M. Dobson, *Nature*, 2003, **426**, 884-890.
895 2. D. Romero, C. Aguilar, R. Losick and R. Kolter, *Proc. Natl. Acad. Sci. U.S.A.*,
896 2010, **107**, 2230-2234.
897 3. C. Dirix, F. Meersman, C. E. MacPhee, C. M. Dobson and K. Heremans, *J.*
898 *Mol. Biol.* , 2005, **347**, 903-909.
899 4. J. Zurdo, J. I. Guijarro and C. M. Dobson, *J. Am. Chem. Soc.*, 2001, **123**,
900 8141-8142.
901 5. J. F. Smith, T. P. J. Knowles, C. M. Dobson, C. E. MacPhee and M. E.
902 Welland, *Proc. Natl. Acad. Sci. U.S.A.*, 2006, **103**, 15806-15811.
903 6. J. Adamcik, C. Lara, I. Usov, J. S. Jeong, F. S. Ruggeri, G. Dietler, H. A.
904 Lashuel, I. W. Hamley and R. Mezzenga, *Nanoscale*, 2012, **4**, 4426-4426.
905 7. T. P. J. Knowles, C. A. Waudby, G. L. Devlin, S. I. A. Cohen, A. Aguzzi, M.
906 Vendruscolo, E. M. Terentjev, M. E. Welland and C. M. Dobson, *Science*,
907 2009, **326**, 1533-1537.
908 8. T. P. Knowles, A. W. Fitzpatrick, S. Meehan, H. R. Mott, M. Vendruscolo, C.
909 M. Dobson and M. E. Welland, *Science* 2007, **318**, 1900-1903.
910 9. M. N. Bongiovanni, D. B. Scanlon and S. L. Gras, *Biomaterials*, 2011, **32**,
911 6099-6110.
912 10. S. L. Gras, A. K. Tickler, A. M. Squires, G. L. Devlin, M. A. Horton, C. M.
913 Dobson and C. E. MacPhee, *Biomaterials*, 2008, **29**, 1553-1562.
914 11. A. J. Baldwin, R. Bader, J. Christodoulou, C. E. MacPhee, C. M. Dobson and
915 P. D. Barker, *Journal of the American Chemical Society*, 2006, **128**, 2162-
916 2163.
917 12. G. Cinar, H. Ceylan, M. Urel, T. S. Erkal, E. Deniz Tekin, A. B. Tekinay, A.
918 Dâna and M. O. Guler, *Biomacromolecules*, 2012, **13**, 3377-3387.
919 13. J. H. Collier, J. S. Rudra, J. Z. Gasiorowski and J. P. Jung, *Chem. Soc. Rev.*,
920 2010, **39**, 3413-3424.
921 14. O. G. Jones and R. Mezzenga, *Soft Matter*, 2012, **8**, 876-895.

15. M. N. Bongiovanni, D. Puri, K. N. Goldie and S. L. Gras, *J. Mol. Biol.* , 2012, **421**, 256-269.
16. J. T. Berryman, S. E. Radford and S. A. Harris, *Biophys. J.*, 2011, **100**, 2234-2242.
17. J.-P. Colletier, A. Laganowsky, M. Landau, M. Zhao, A. B. Soriaga, L. Goldschmidt, D. Flot, D. Cascio, M. R. Sawaya and D. Eisenberg, *Proc. Natl. Acad. Sci. U.S.A.*, 2011.
18. J. Madine, E. Jack, P. G. Stockley, S. E. Radford, L. C. Serpell and D. A. Middleton, *J. Am. Chem. Soc.*, 2008, **130**, 14990-15001.
19. J. Meinhardt, C. Sachse, P. Hortschansky, N. Grigorieff and M. Fändrich, *J. Mol. Biol.*, 2009, **386**, 869-877.
20. K. E. Marshall, K. L. Morris, D. Charlton, N. O'Reilly, L. Lewis, H. Walden and L. C. Serpell, *Biochemistry*, 2011, **50**, 2061-2071.
21. M. Reches, Y. Porat and E. Gazit, *J. Biol. Chem.*, 2002, **277**, 35475-35480.
22. S. Nath, J. Goodwin, Y. Engelborghs and D. L. Pountney, *Mol. Cell. Neurosci.*, 2011, **46**, 516-526.
23. M. S. Dueholm, S. B. Nielsen, K. L. Hein, P. Nissen, M. Chapman, G. Christiansen, P. H. Nielsen and D. E. Otzen, *Biochemistry*, 2011, **50**, 8281-8290.
24. K. Klement, K. Wieligmann, J. Meinhardt, P. Hortschansky, W. Richter and M. Fändrich, *J. Mol. Biol.*, 2007, **373**, 1321-1333.
25. B. Raman, E. Chatani, M. Kihara, T. Ban, M. Sakai, K. Hasegawa, H. Naiki, C. M. Rao and Y. Goto, *Biochemistry*, 2005, **44**, 1288-1299.
26. M. Muzaffar and A. Ahmad, *PLoS ONE*, 2011, **6**, e27906-e27906.
27. L. A. Sikkink and M. Ramirez-Alvarado, *Biophys. Chem.*, 2008, **135**, 25-31.
28. P. Lo Nostro and B. W. Ninham, *Chem. Rev.*, 2012, **112**, 2286-2322.
29. Y. Zhang and P. S. Cremer, *Proceedings of the National Academy of Sciences*, 2009, **106**, 15249-15253.
30. J. S. Pedersen, J. M. Flink, D. Dikov and D. E. Otzen, *Biophys. J.*, 2006, **90**, 4181-4194.
31. S. Jain and J. B. Udgaonkar, *Biochemistry*, 2010, **49**, 7615-7624.
32. L. A. Munishkina, J. Henriques, V. N. Uversky and A. L. Fink, *Biochemistry*, 2004, **43**, 3289-3300.
33. V. Yeh, J. M. Broering, A. Romanyuk, B. Chen, Y. O. Chernoff and A. S. Bommarius, *Protein Sci.*, 2010, **19**, 47-56.
34. S. M. Loveday, J. Su, M. A. Rao, S. G. Anema and H. Singh, *Int. Dairy J.* , 2012, **26**, 133-140.
35. S. M. Loveday, X. L. Wang, M. A. Rao, S. G. Anema, L. K. Creamer and H. Singh, *Int. Dairy J.*, 2010, **20**, 571-579.
36. P. J. Marek, V. Patsalo, D. F. Green and D. P. Raleigh, *Biochemistry*, 2012, **51**, 8478-8490.
37. J. Adamcik and R. Mezzenga, *Soft Matter*, 2011, **7**, 5437-5443.
38. C. P. Jaroniec, C. E. MacPhee, N. S. Astrof, C. M. Dobson and R. G. Griffin, *Proc. Natl. Acad. Sci. U.S.A.*, 2002, **99**, 16748-16753.
39. M. A. Caporini, V. S. Bajaj, M. Veshtort, A. Fitzpatrick, C. E. MacPhee, M. Vendruscolo, C. M. Dobson and R. G. Griffin, *J Phys Chem. B.*, 2010, **114**, 13555-13561.
40. A. Udomprasert, M. N. Bongiovanni, R. Sha, W. B. Sherman, P. Arora, J. W. Canary, S. L. Gras and N. C. Seeman, *unpublished data*, 2012.

41. S. Bulut, T. S. Erkal, S. Toksoz, A. B. Tekinay, T. Tekinay and M. O. Guler, *Biomacromolecules*, 2011, **12**, 3007-3014.
42. E. Gasteiger, C. Hoogland, A. Gattiker, S. Duvand, M. Wilkins, R. Appel and A. Bairoch, *Protein identification and analysis tools on the ExPASy server*, Humana Press Inc., Totowa, New Jersey, 2005.
43. A. Gustavsson, U. Engstrom and P. Westermark, *Biochem. Biophys. Res. Commun.*, 1991, **175**, 1159-1164.
44. G. T. Hermanson, *Bioconjugate Techniques, Second Edition*, Academic Press, 2008.
45. A. G. Street and S. L. Mayo, *Proc. Natl. Acad. Sci. U.S.A.*, 1999, **96**, 9074-9076.
46. E. Paci, J. Gsponer, X. Salvatella and M. Vendruscolo, *Journal of Molecular Biology*, 2004, **340**, 555-569.
47. S. Maurer-Stroh, M. Debulpaep, N. Kuemmerer, M. Lopez de la Paz, I. C. Martins, J. Reumers, K. L. Morris, A. Copland, L. Serpell, L. Serrano, J. W. H. Schymkowitz and F. Rousseau, *Nat. Methods*, 2010, **7**, 237-242.
48. A.-M. Fernandez-Escamilla, F. Rousseau, J. Schymkowitz and L. Serrano, *Nature Biotechnology*, 2004, **22**, 1302-1306.
49. O. Conchillo-Solé, N. S. de Groot, F. X. Avilés, J. Vendrell, X. Daura and S. Ventura, *BMC Bioinformatics*, 2007, **8**, 65-65.
50. G. G. Tartaglia, A. P. Pawar, S. Campioni, C. M. Dobson, F. Chiti and M. Vendruscolo, *Journal of Molecular Biology*, 2008, **380**, 425-436.
51. C. Blake and L. Serpell, *Structure*, 1996, **4**, 989-998.
52. S. Udenfriend, S. Stein, P. Böhlen, W. Dairman, W. Leimgruber and M. Weigele, *Science*, 1972, **178**, 871-872.
53. A. J. Baldwin, T. P. J. Knowles, G. G. Tartaglia, A. W. Fitzpatrick, G. L. Devlin, S. L. Shammas, C. A. Waudby, M. F. Mossuto, S. Meehan, S. L. Gras, J. Christodoulou, S. J. Anthony-Cahill, P. D. Barker, M. Vendruscolo and C. M. Dobson, *J. Am. Chem. Soc.*, 2011, **133**, 14160-14163.
54. T. Scheibel, A. S. Kowal, J. D. Bloom and S. L. Lindquist, *Curr. Biol.*, 2001, **11**, 366-369.
55. C. C. Vandenakker, M. F. M. Engel, K. P. Velikov, M. Bonn and G. H. Koenderink, *J. Am. Chem. Soc.*, 2011, **133**, 18030-18033.
56. S. I. A. Cohen, M. Vendruscolo, C. M. Dobson and T. P. J. Knowles, *Int. J. Mol. Sci.*, 2011, **12**, 5844-5852.
57. C. P. Jaroniec, C. E. MacPhee, N. S. Astrof, C. M. Dobson and R. G. Griffin, *Proceedings of the National Academy of Sciences of the United States of America*, 2002, **99**, 16748-16753.
58. P. Hortschansky, V. Schroeckh, T. Christopeit, G. Zandomeneghi and M. Fändrich, *Protein Sci.*, 2005, **14**, 1753-1759.
59. S. H. White and W. C. Wimley, *Biochim. Biophys. Acta*, 1998, **1376**, 339-352.
60. K. F. DuBay, A. P. Pawar, F. Chiti, J. Zurdo, C. M. Dobson and M. Vendruscolo, *J. Mol. Biol.*, 2004, **341**, 1317-1326.
61. B. Morel, L. Varela, A. I. Azuaga and F. Conejero-Lara, *Biophys. J.*, 2010, **99**, 3801-3810.
62. P. Lo Nostro, N. Peruzzi, M. Severi, B. W. Ninham and P. Baglioni, *J. Am. Chem. Soc.*, 2010, **132**, 6571-6577.
63. M. Calamai, N. Taddei, M. Stefani, G. Ramponi and F. Chiti, *Biochemistry*, 2003, **42**, 15078-15083.

64. M. López De La Paz, K. Goldie, J. Zurdo, E. Lacroix, C. M. Dobson, A. Hoenger and L. Serrano, *Proc. Natl. Acad. Sci. U.S.A.*, 2002, **99**, 16052-16057.
65. Y. Zhang and P. S. Cremer, *Annu. Rev. Phys. Chem.*, 2010, **61**, 63-83.
66. D. T. Gjerde, G. Schmuckler and J. S. Fritz, *J. Chromatrgr. A*, 1980, **187**, 35-45.
67. J. Adamcik and R. Mezzenga, *Curr. Opin. Colloid Interface Sci.*, 2012, **17**, 369-376.
68. N. J. Greenfield and G. D. Fasman, *Biochemistry*, 1969, **8**, 4108-4116.
69. I. W. Hamley, G. D. Brown, V. Castelletto, G. Cheng, M. Venanzi, M. Caruso, E. Placidi, C. Aleman, G. Revilla-López and D. Zanuy, *J. Phys. Chem. B*, 2010, **114**, 10674-10683.
70. J. Kyte and R. F. Doolittle, *J. Mol. Biol.*, 1982, **157**, 105-132.
71. F. Chiti, M. Stefani, N. Taddei, G. Ramponi and C. M. Dobson, *Nature*, 2003, **424**, 805-808.
72. R. L. Schowen, *J. Chem. Educ.*, 2011, **70**, A223-A223.
73. C. Tanford and J. G. Kirkwood, *J. Am. Chem. Soc.*, 2011, **79**, 5333-5339.
74. T. M. McPhillips, S. E. McPhillips, H. J. Chiu, A. E. Cohen, A. M. Deacon, P. J. Ellis, E. Garman, A. Gonzalez, N. K. Sauter, R. P. Phizackerley, S. M. Soltis and P. Kuhn, *J. Synchrotron Radiat.*, 2002, **9**, 401-406.
75. A. M. Squires, G. L. Devlin, S. L. Gras, A. K. Tickler, C. E. MacPhee and C. M. Dobson, *J. Am. Chem. Soc.*, 2006, **128**, 11738-11739.

Table 1. The effect of solution conditions including salt ions, pH and changes in ionic strength on the formation of TTR1-GGK fibrils as assessed by the kinetic parameters elongation rate (k (h^{-1})) and lag time (t_l (h)).

Sample	Lag time t_l (h)	Fibril longation rate k (h^{-1})
Unseeded	17 ± 3.1	0.70 ± 0.3
Seeded	0.2 ± 0.0	4.2 ± 0.1
500 mM NaCl	2.1 ± 0.7	0.33 ± 0.0
250 mM NaCl	4.0 ± 1.5	0.55 ± 0.1
100 mM NaCl	4.9 ± 1.7	0.74 ± 0.0
NaCl	10 ± 1.2	1.5 ± 0.1
$CaCl_2$	4.1 ± 1.0	0.91 ± 0.0
$CaCl_2$ pH 6.5	2.4 ± 0.1	0.91 ± 0.0
CaCl2 pH 10.5	4.2 ± 1.6	0.76 ± 0.1
$MgCl_2$	6.8 ± 0.5	1.1 ± 0.0
KCl	8.1 ± 0.2	1.5 ± 0.1
LiCl	7.2 ± 0.5	1.9 ± 0.3
NaI	2.4 ± 0.1	1.5 ± 0.1
$NaNO_3$	2.7 ± 0.1	0.88 ± 0.1
Na_2SO_4	2.9 ± 0.6	1.6 ± 0.2

Data were obtained by fitting a sigmoidal curve to the turbidity data measured at 330 nm to assess fibril formation. Fibrils were formed at pH 2.0 and a salt concentration of 50 mM was used unless otherwise stated. The data presented are the mean from at least 4 measurements and the error is the standard deviation. Unseeded fibrils were formed in a solution of 10% (v/v) CH_3CN. Seeded fibril formation involved the addition of 5% (v/v) fragmented mature fibrils.

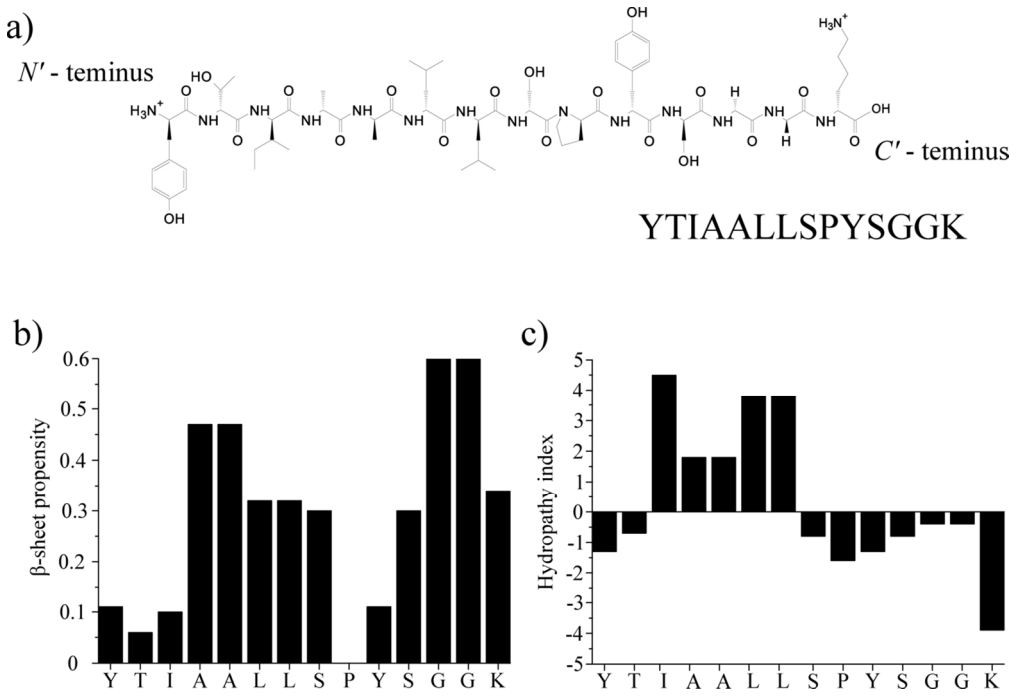

Figure 1. Bioinformatic analysis of the TTR1-GGK peptide sequence. a) Chemical structure of the TTR1-GGK peptide and single amino acid code. b) β-sheet propensity of each residue determined by the Street and Mayo scale. c) The hydropathy of each residue determined by the Kyte and Doolittle index, where a positive value denotes a hydrophobic residue.
125x85mm (300 x 300 DPI)

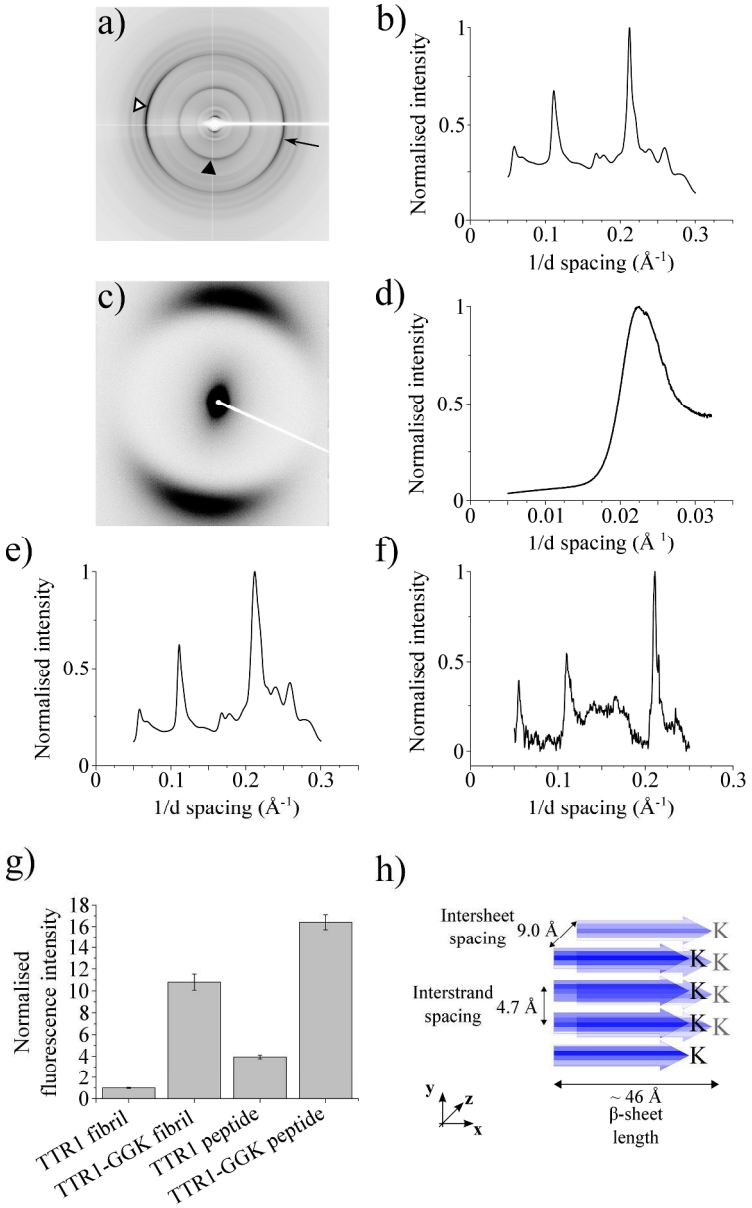

Figure 2. Structural analysis of TTR1-GGK fibrils assembled in 10% (v/v) CH_3CN. a) WAXS 2D diffraction pattern and b) the corresponding normalised WAXS 1D profile from a dried fibril stalk of unseeded TTR1-GGK fibrils. The open and closed triangles indicate major anisotropic reflections at ~4.7 Å and ~9.0 Å respectively in the 2D pattern. The arrow indicates the axis of the fibril. c) SAXS 2D diffraction pattern and d) the corresponding normalised SAXS 1D profile from the same dried fibril stalk of unseeded TTR1-GGK fibrils. Normalised WAXS 1D profiles e) from a dried stalk of seeded TTR1-GGK fibrils and f) from a hydrated pellet of TTR1-GGK fibrils. g) Fluorescent assay to detect primary amines accessible on the surface of TTR1 or TTR1-GGK fibrils or TTR1 or TTR1-GGK peptides. The data presented is the mean ± SD of eight replicates. h) A schematic representation of the proposed core structure within TTR1-GGK fibrils, where the arrows indicate the likely arrangement of the TTR1-GGK peptide within the cross-β core.
218x354mm (300 x 300 DPI)

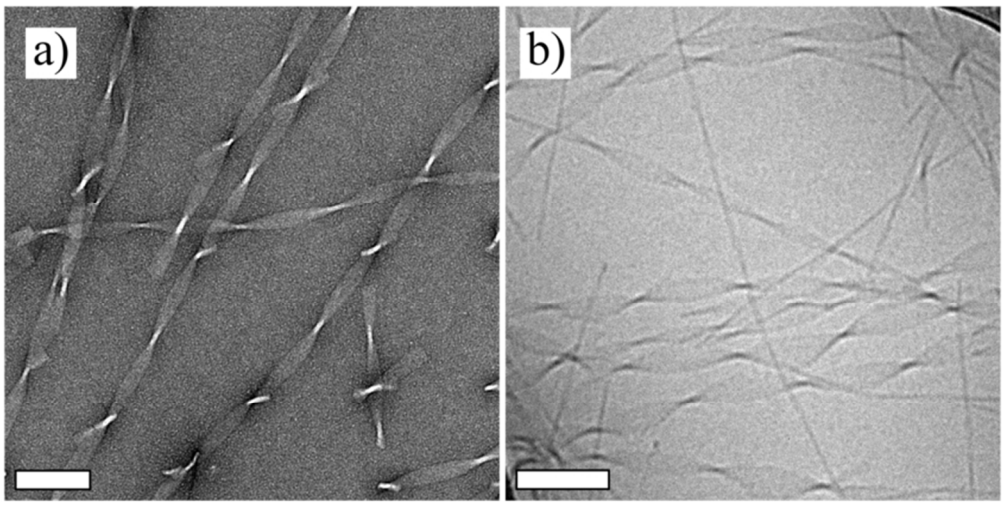

Figure 3. The morphology of TTR1-GGK fibrils assembled in 10% (v/v) CH_3CN. Transmission electron micrographs of mature fibrils a) dried and negatively stained with uranyl acetate 2% (w/v) or b) cryo-preserved. The scale bars are 100 nm in length.
71x35mm (300 x 300 DPI)

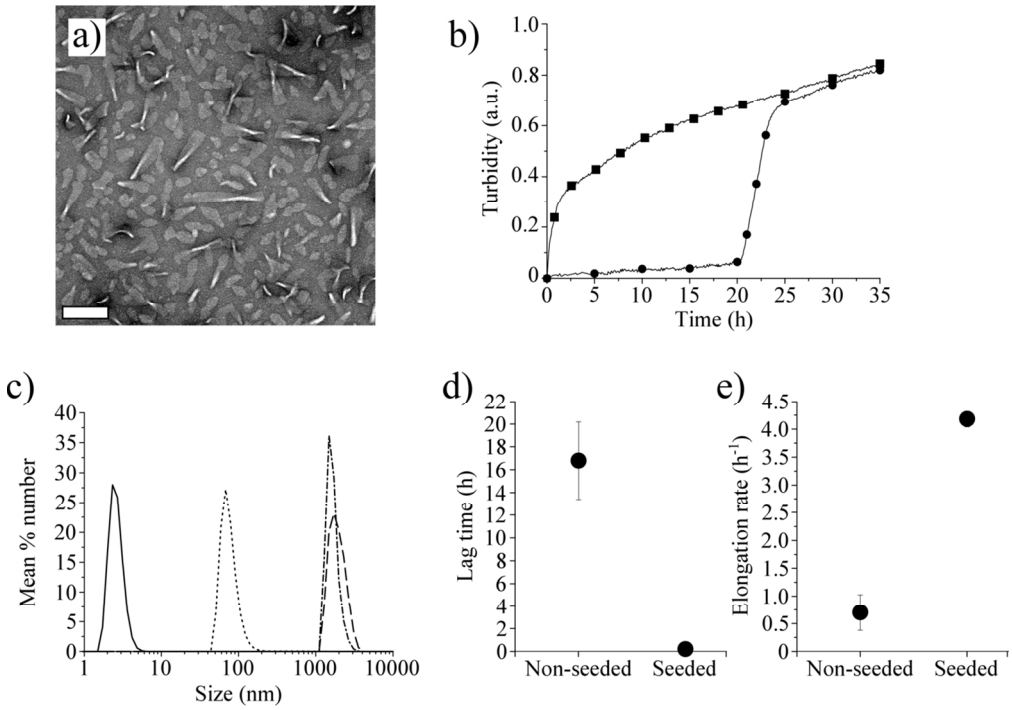

Figure 4. The kinetics of TTR1-GGK fibril formation in 10% (v/v) CH_3CN at pH 2.0. a) TEM image of the fragmented mature fibrils used for seeding fibril growth. The scale bar is 100 nm in length. b) An example of solution turbidity (330 nm) of the TTR1-GGK peptide measured over time for unseeded peptide (circles) or peptide seeded with 5% (v/v) fragmented mature fibrils (squares). c) Dynamic light scattering data obtained from freshly dissolved TTR1-GGK peptide (solid line), fragmented mature TTR1-GGK fibrils used as seeds (dotted line), unseeded TTR1-GGK peptide after 24 hours of incubation (dot-dash-dot line) or seeded TTR1-GGK peptide (dashed line) after 24 hours of incubation. The kinetic parameters of TTR1-GGK fibril formation determined from turbidity measurements represented in b): d) lag time t_l (h) and e) the elongation rate k (h^{-1}). Data are the mean ± SD (n = 5), note the variability is much less in seeded samples.
124x87mm (300 x 300 DPI)

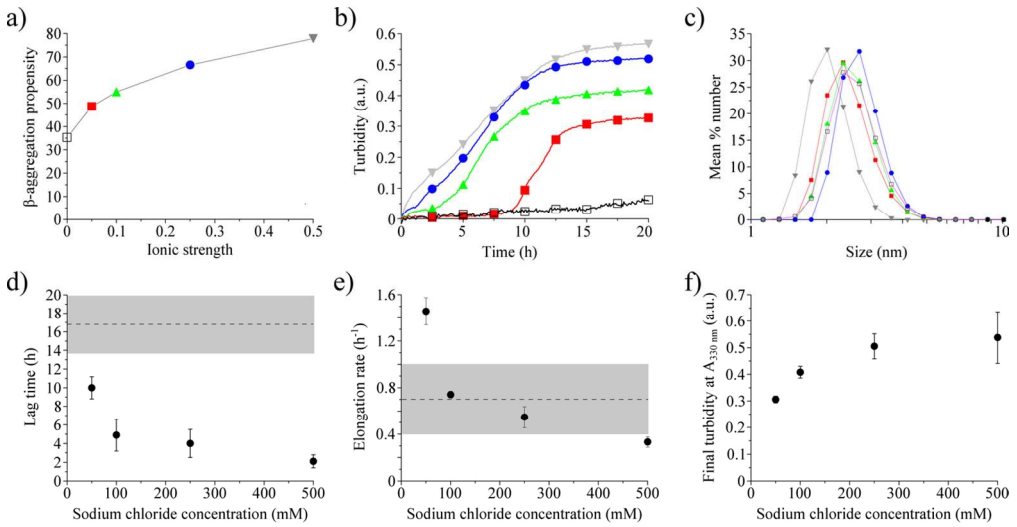

Figure 5. The effect of sodium chloride (NaCl) addition on the kinetics of TTR1-GGK fibril assembly. a) The β-aggregation propensity of the TTR1-GGK peptide as predicted by the TANGO algorithm for solutions of increasing ionic strength at pH 2.0. b) An example of solution turbidity (330 nm) of the TTR1-GGK peptide measured over time for peptide in 10% (v/v) CH_3CN (open square) or in NaCl salt at various concentrations in water; 50 mM (closed square), 100 mM (triangle), 250 mM (circle) and 500 mM (inverted triangle). These NaCl concentrations correspond to four ionic strengths used for the TANGO predictions in 5a). c) Dynamic light scattering data obtained from solutions of the TTR1-GGK peptide in water with various concentrations of NaCl; the symbols represent the same concentrations as in b). d-f) Kinetic parameters calculated from turbidity measurements shown in 5b): d) lag time (t_l (h)), e) elongation rate (k (h^{-1}) and f) final turbidity, where the data is the mean ± SD and n = 4. The dashed line and shaded region in d) and e) indicate the mean ± SD respectively for the kinetics of TTR1-GGK fibril assembly in 10% (v/v) CH_3CN.
128x66mm (300 x 300 DPI)

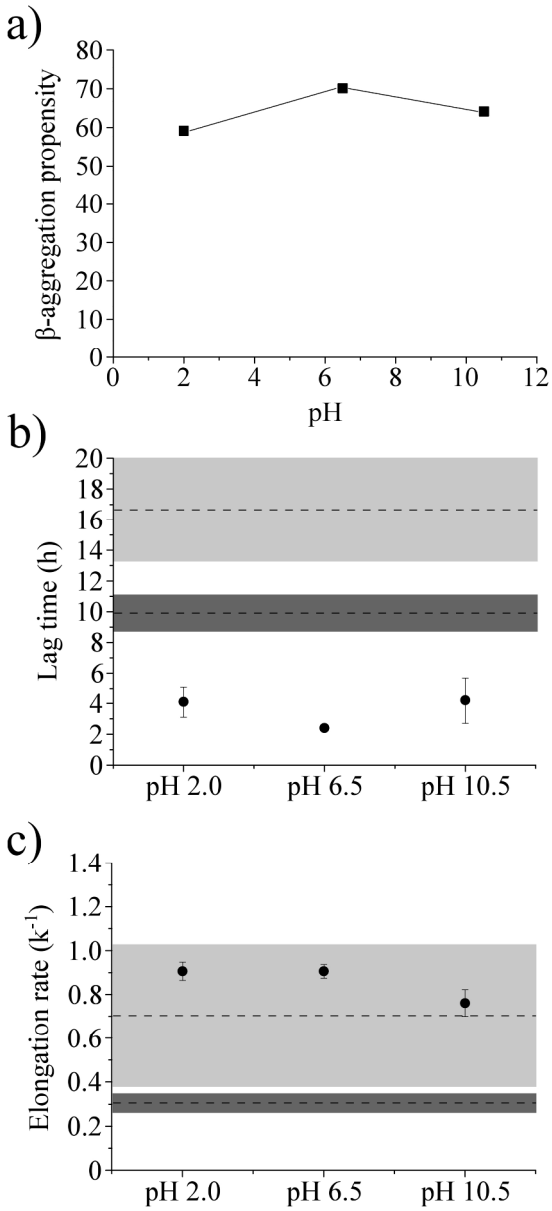

Figure 6. The effect of calcium chloride ($CaCl_2$) addition and solution pH on the kinetics of TTR1-GGK fibril assembly. a) The β-aggregation propensity of the TTR1-GGK peptide, as predicted by the TANGO algorithm as a function of solution pH. The ionic strength was constant with 50 mM $CaCl_2$ added to all solutions. Experimentally determined kinetic parameters for TTR1-GGK fibril formation in solutions of varying pH: b) lag time t_l (h) and c) elongation rate k (h^{-1}), where the data are the mean ± SD and n = 4. The dashed line and shaded region in b) and c) indicate the mean ± SD respectively for the kinetics of TTR1-GGK fibril assembly in 10% (v/v) CH_3CN (grey) and in 50 mM NaCl (dark grey).
169x375mm (300 x 300 DPI)

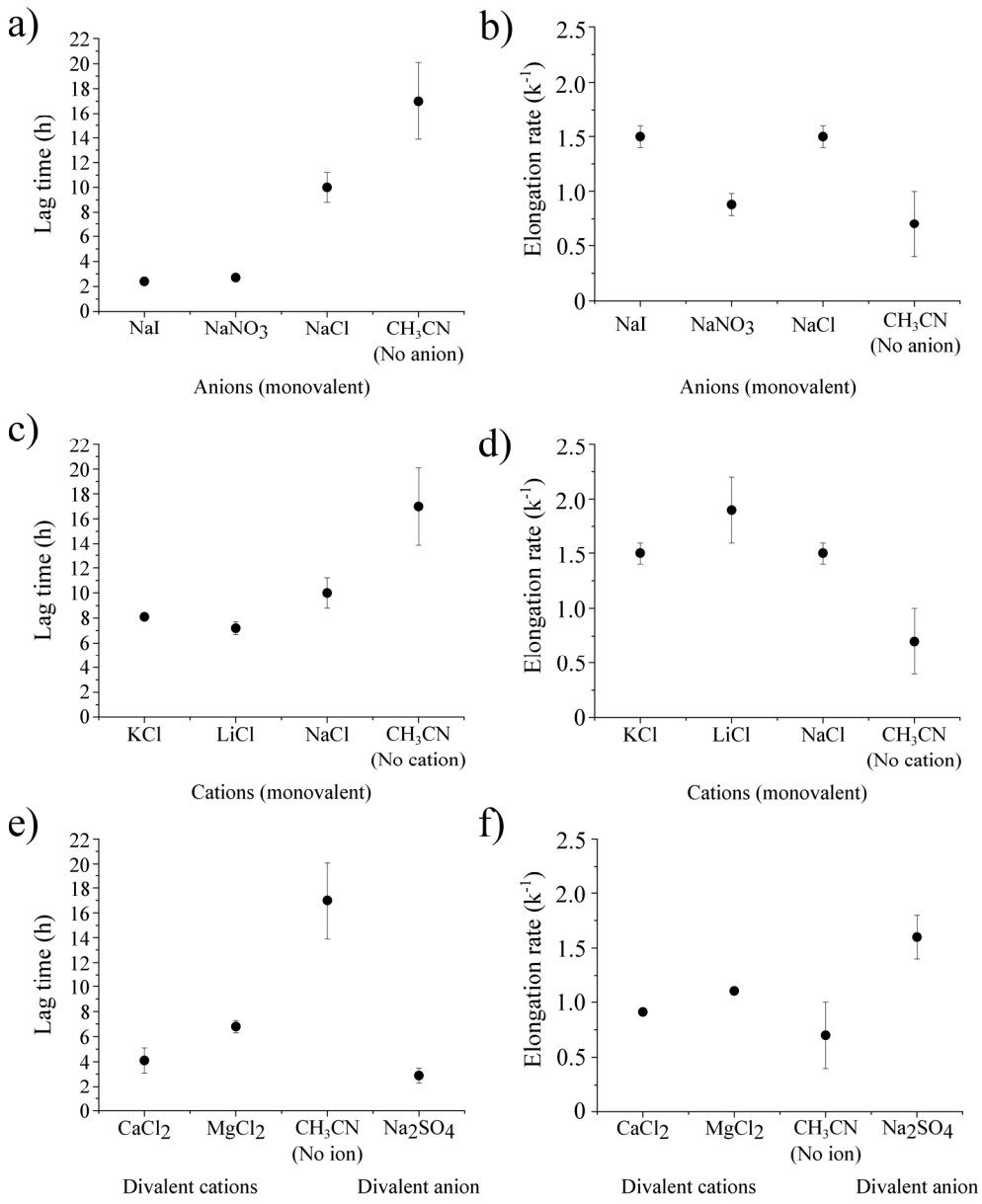

Figure 7. The effect of the addition of a range of salts on the kinetics of TTR1-GGK fibril formation. All salts were added at 50 mM and the solution pH was 2.0. The effect of different monovalent sodium paired anions (total solution ionic strength of 50 mM) on: a) lag time t_l (h) and b) the elongation rate k (h^{-1}). The effect of different monovalent chloride paired cations (total solution ionic strength of 50 mM) on: c) lag time t_l (h) and d) the elongation rate k (h^{-1}). The effect of different divalent cations and an anion (total ionic strength 130 mM) on : e) lag time t_l (h) and f) the elongation rate k (h^{-1}). All data are the mean ± SD and n = 4.
193x236mm (300 x 300 DPI)

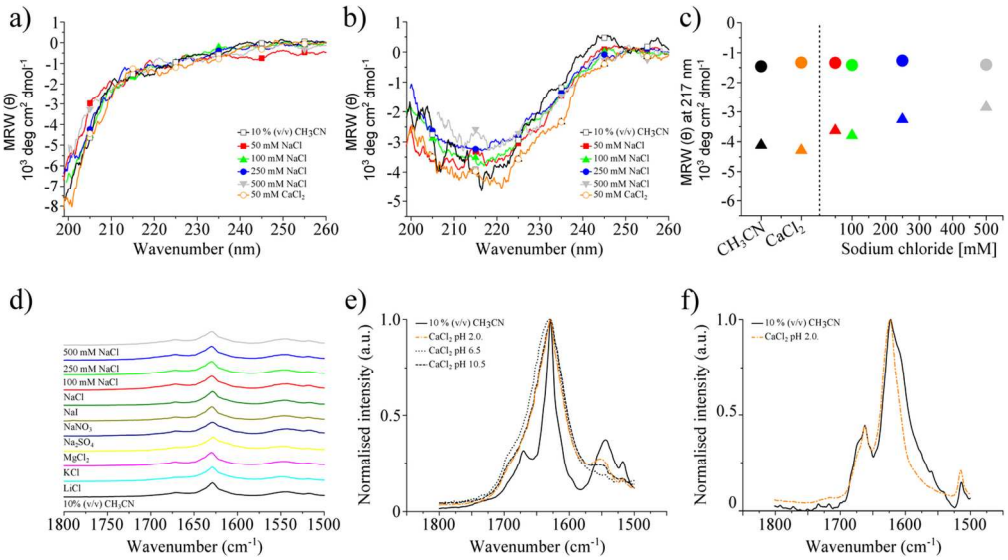

Figure 8. Analysis of secondary structure for the TTR1-GGK peptide and fibrils. Circular dichroism spectra of: a) the TTR1-GGK peptide or b) TTR1-GGK fibrils as a function of NaCl concentration (50 mM, 100 mM, 250 mM or 500 mM) or 50 mM $CaCl_2$ addition at pH 2.0. c) The mean residue ellipticity (MRW[θ]) measured at a wavenumber of 217 nm for the solutions of the TTR1-GGK peptide (circles) or TTR1-GGK fibril (triangles) with various salt concentrations corresponding to the conditions in a) and b). d) ATR-FTIR spectra for a hydrated film of TTR1-GGK fibrils in the presence of various salts at 50 mM or NaCl at varying concentrations at pH 2.0. e) The amide I region of the ATR-FTIR spectra for TTR1-GGK fibrils in the presence of 10% (v/v) CH_3CN or 50 mM $CaCl_2$ at a range of pH: 2.0, 6.5 or 10.5. f) Transmission-FTIR spectra for TTR1-GGK fibrils in D_2O with 10% (v/v) CH_3CN or the addition of 50 mM $CaCl_2$. Both solutions are at pH 2.0. All IR spectra are normalised to the highest intensity of the major amide I peak in each spectrum.
128x70mm (300 x 300 DPI)

Supplementary Information

Supplementary figures

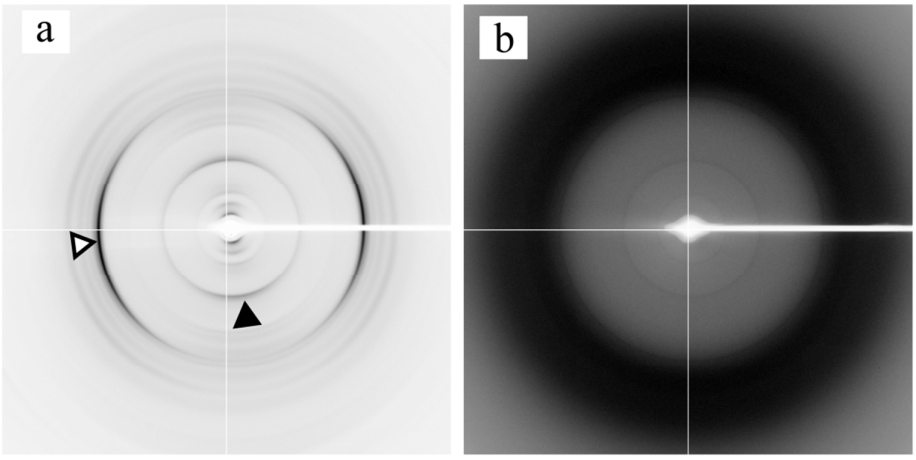

SI Figure 1: WAXS 2D patterns obtained from TTR1-GGK fibrils using a) a dried stalk of seeded TTR1-GGK fibrils or b) a hydrated pellet of TTR1-GGK fibrils. The open and closed triangles indicate major anisotropic reflections at 4.7 Å and 9.0 Å respectively.

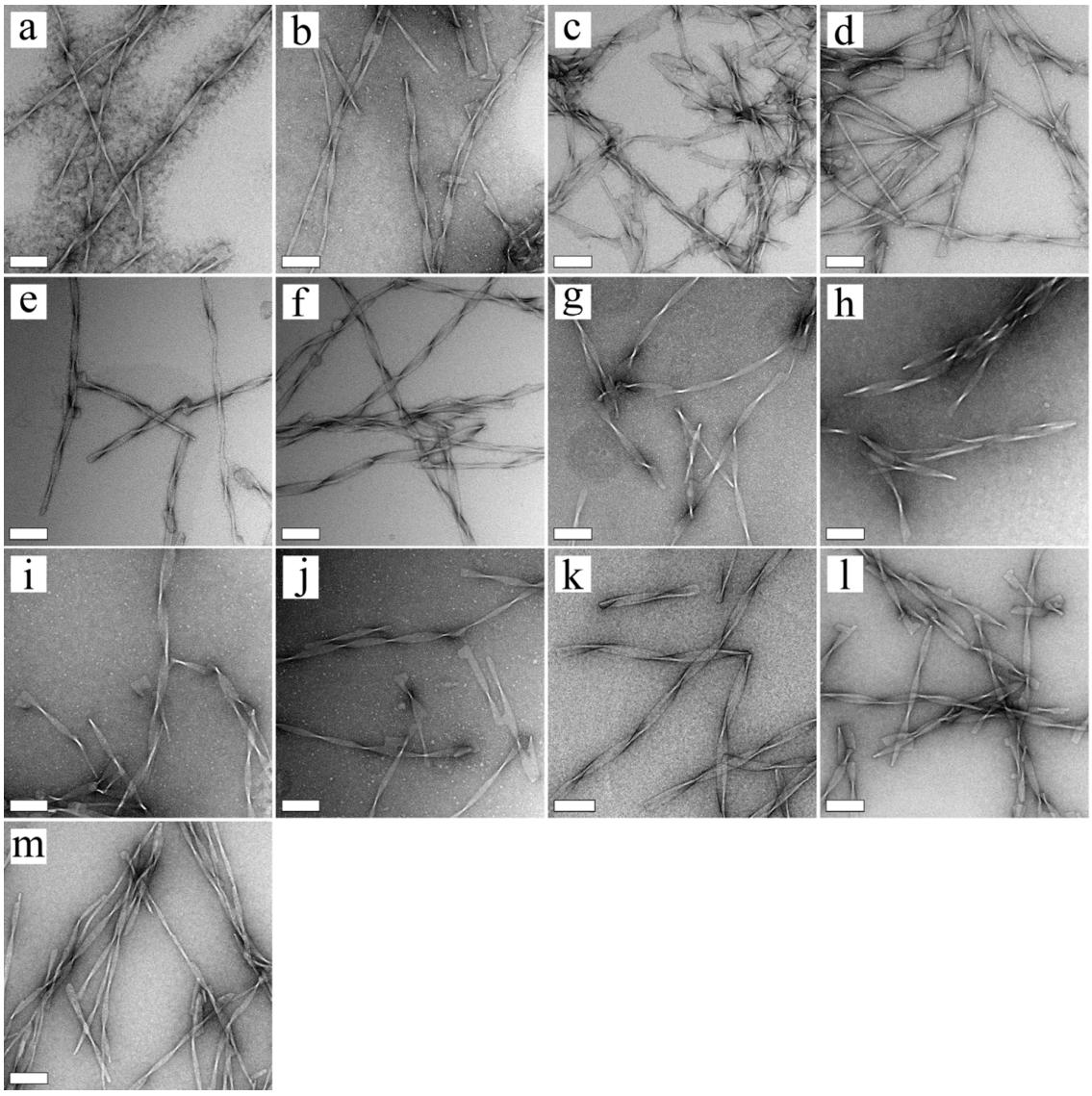

SI Figure 2: Transmission electron microscopy images of mature fibrils assembled from the TTR1-GGK peptide in different solution conditions at pH 2.0 unless otherwise stated containing: a) 50 mM NaCl, b) 100 mM NaCl, c) 250 mM NaCl, d) 500 mM NaCl, e) 50 mM LiCl, f) 50 mM KCl, g) 50 mM $MgCl_2$, h) 50 mM Na_2SO_4, i) 50 mM $NaNO_3$, j) 50 mM NaI, k) 50 mM $CaCl_2$, l) 50 mM $CaCl_2$ at pH 6.5 or m) 50 mM $CaCl_2$ at pH 10.5. The scale bars are all 100 nm in length.

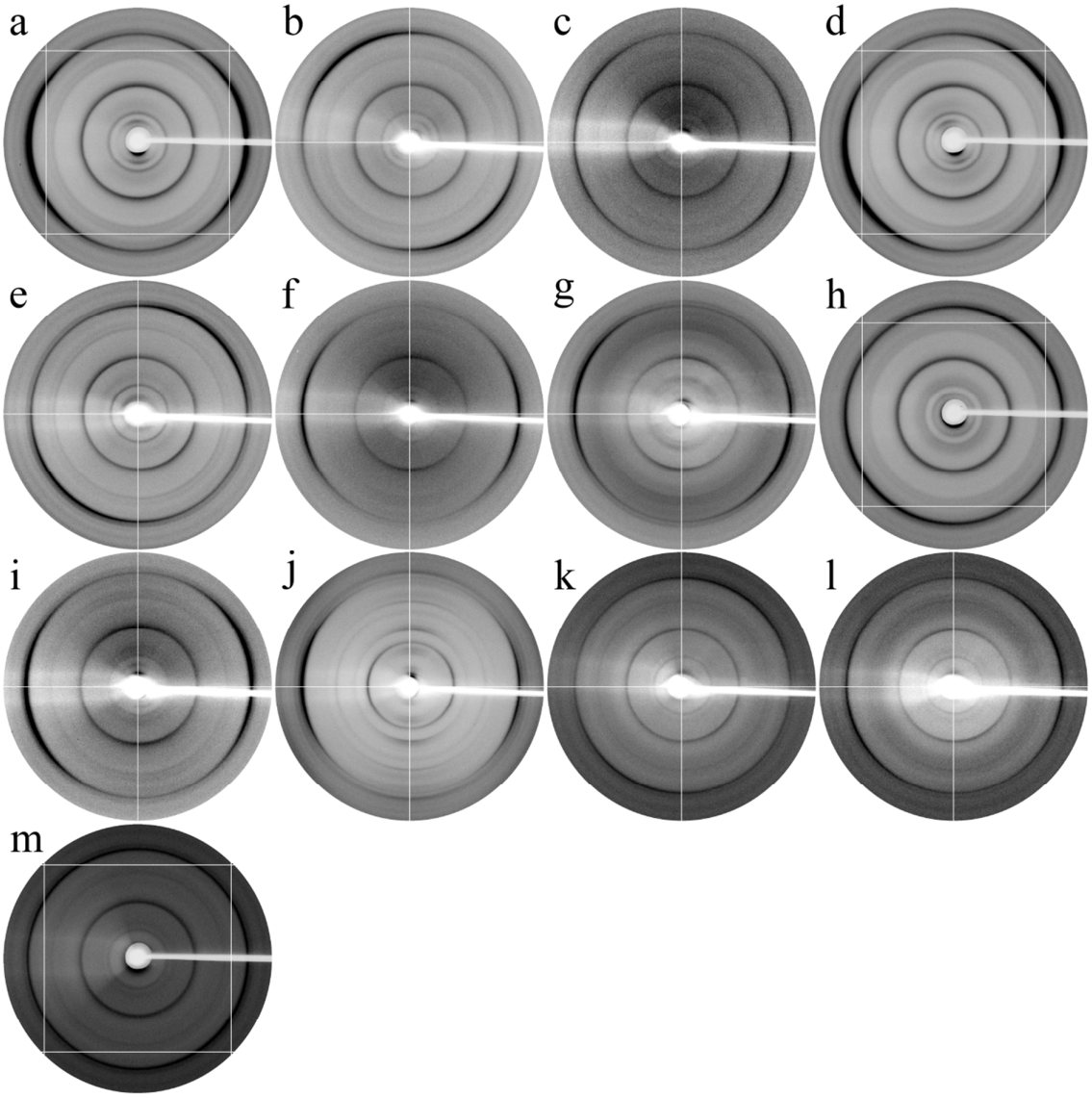

SI Figure 3: WAXS 2D diffraction patterns obtained from dried stalks of fibrils assembled in different solution conditions at pH 2.0 unless otherwise stated: a) 50 mM NaCl, b) 100 mM NaCl, c) 250 mM NaCl, d) 500 mM NaCl, e) 50 mM LiCl , f) 50 mM KCl, g) 50 mM $MgCl_2$, h) 50 mM Na_2SO_4, i) 50 mM $NaNO_3$, j) 50 mM NaI, k) 50 mM $CaCl_2$, l) 50 mM $CaCl_2$ at pH 6.5 and m) 50 mM $CaCl_2$ at pH 10.5. The white lines arise from the X-ray detectors used.

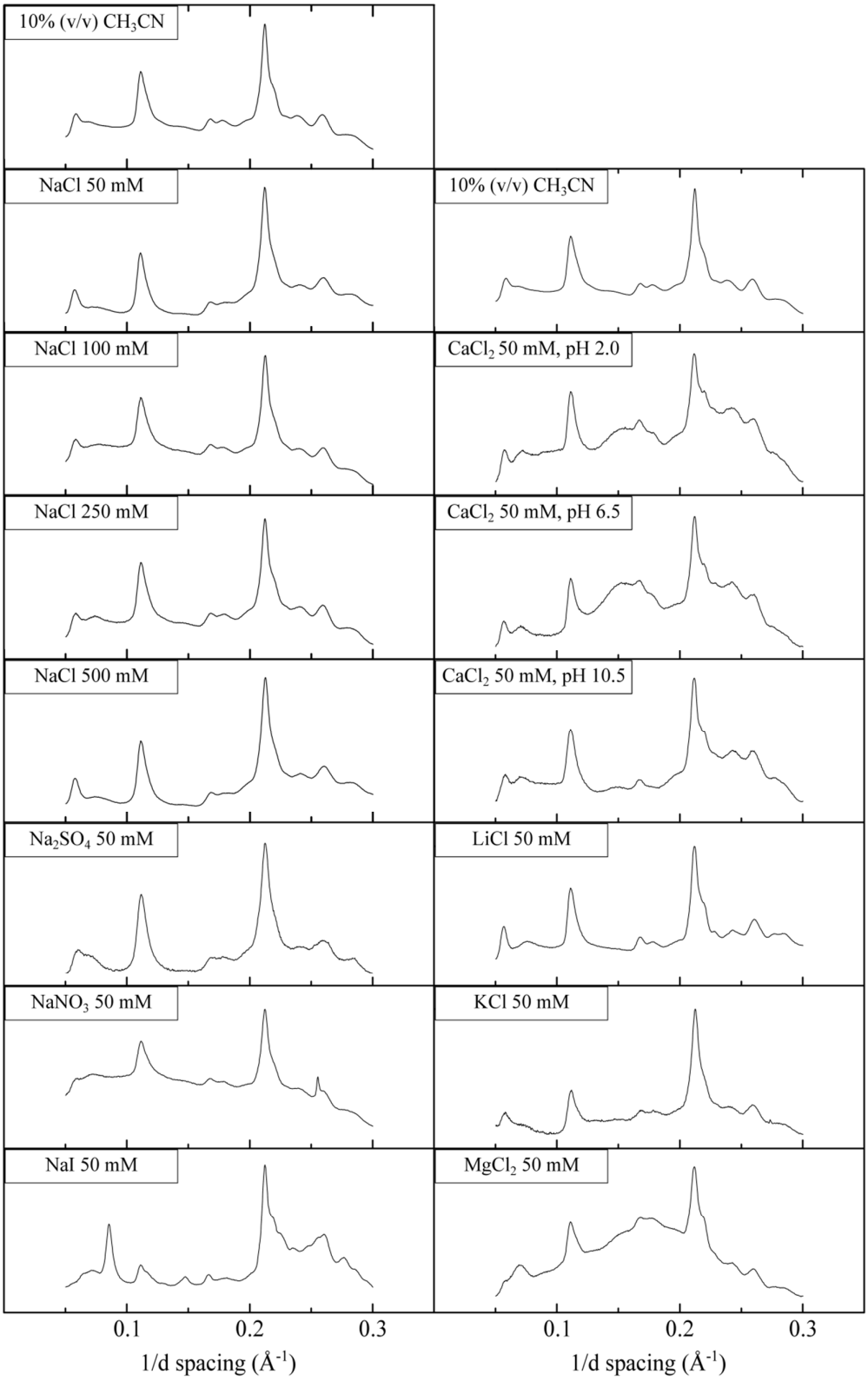

SI Figure 4: Normalised WAXS 1D profiles obtained from dried stalks. The data corresponds to the diffraction patterns shown in SI Figure 3. The pattern obtained from fibrils assembled in 10% (v/v) CH_3CN is added to each column for comparison.

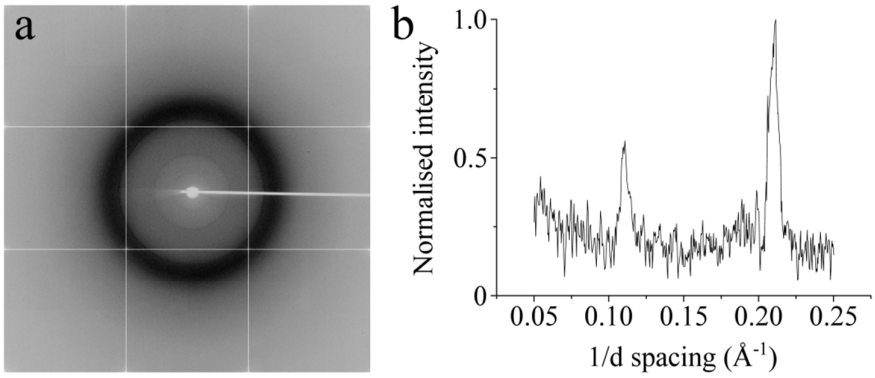

SI Figure 5: a) WAXS 2D diffraction pattern for a hydrated pellet of TTR1-GGK fibrils assembled in the presence of 50 mM $CaCl_2$ at pH 2.0 and b) corresponding WAXS 1D profile.

The pitch of TTR1-GGK fibrils assembled in under each of the conditions listed in SI Table 3 was measured within TEM images using the ImageJ software (NIH, Bethesda, MD, USA). The pixel size was calibrated using the imprinted scale bar. An example of the fibril pitch is given in SI Figure 6b. The measured pitch for each conditions is given in SI Table 3.

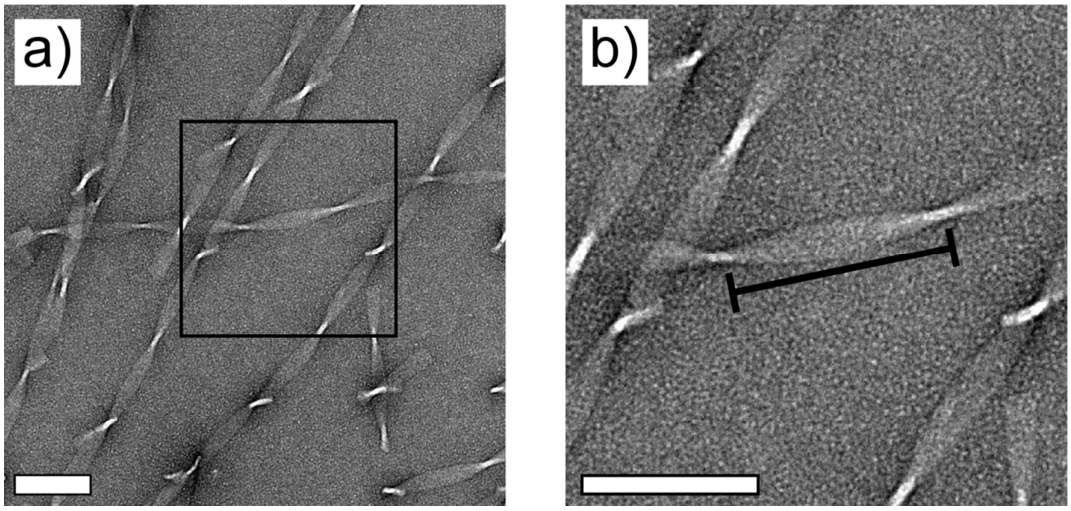

SI Figure 6: TEM image of TTR1-GGK fibrils. b) Magnified TEM image of the square section in a). The pitch of the fibrils was measured as indicated by the black bar.

Supplementary Tables

SI Table 1: Position of the major amide I peak in ATR-FTIR spectra for a hydrated layer of TTR1-GGK fibrils.

Sample [a]	Position of amide I main peak [cm^{-1}]
Unseeded [b]	1629
500 mM NaCl	1630
250 mM NaCl	1630
100 mM NaCl	1630
NaCl	1630
$CaCl_2$	1629
$CaCl_2$ pH 6.5	1631
CaCl2 pH 10.5	1631
$MgCl_2$	1628
KCl	1630
LiCl	1629
NaI	1629
$NaNO_3$	1630
Na_2SO_4	1630

[a] Fibrils were formed at pH 2.0 unless otherwise stated. The salt concentration used was 50 mM unless otherwise stated. [b] Unseeded fibril formation was in a solution of 10% (v/v) CH_3CN at pH 2.0.

SI Table 2: Position of maxima in WAXS diffraction patterns for TTR1-GGK fibrils assembled in different solution conditions corresponding to the spacing between β-strands and β-sheets.

Sample	Inter-strand spacing [Å]	Inter-sheet spacing [Å]
Unseeded [a]	4.71 ± 0.01	8.99 ± 0.03
Seeded [a]	4.72 ± 0.01	9.00 ± 0.02
Hydrated pellet [a]	4.74 ± 0.03	9.11 ± 0.07
500 mM NaCl	4.71 ± 0.01	8.96 ± 0.01
250 mM NaCl	4.71 ± 0.01	8.98 ± 0.01
100 mM NaCl	4.70 ± 0.03	8.97 ± 0.03
NaCl	4.71 ± 0.02	8.96 ± 0.02
$CaCl_2$	4.72 ± 0.01	8.98 ± 0.06
$CaCl_2$ hydrated pellet	4.74 ± 0.01	9.01 ± 0.02
$CaCl_2$ pH 6.5	4.72 ± 0.01	8.98 ± 0.02
CaCl2 pH 10.5	4.72 ± 0.02	9.00 ± 0.03
$MgCl_2$	4.72 ± 0.01	9.00 ± 0.04
KCl	4.71 ± 0.01	8.95 ± 0.02
LiCl	4.72 ± 0.01	9.02 ± 0.01
NaI	4.74 ± 0.01	8.96 ± 0.02
$NaNO_3$	4.71 ± 0.01	8.99 ± 0.04
Na_2SO_4	4.71 ± 0.01	8.95 ± 0.03

[a] Fibrils were assembled in 10% (v/v) CH_3CN. The solution was at pH 2.0 at a salt concentration of 50 mM unless otherwise stated.

SI Table 3: TTR1-GGK fibril pitch length measured from TEM images as described above. Data is the mean ± S.D. (n = 50).

Sample [a]	Pitch length [nm]
Unseeded [b]	132 ± 6
500 mM NaCl	110 ± 15
250 mM NaCl	115 ± 28
100 mM NaCl	114 ± 12
NaCl	131 ± 19
$CaCl_2$	150 ± 35
$CaCl_2$ pH 6.5	124 ± 14
CaCl2 pH 10.5	120 ± 17
$MgCl_2$	122 ± 11
KCl	118 ± 19
LiCl	108 ± 11
NaI	135 ± 17
$NaNO_3$	128 ± 18
Na_2SO_4	132 ± 29

[a] Fibrils were formed at pH 2.0 unless otherwise stated. The salt concentration used was 50 mM unless otherwise stated. [b] Unseeded fibril formation was in a solution of 10% (v/v) CH_3CN at pH 2.0.

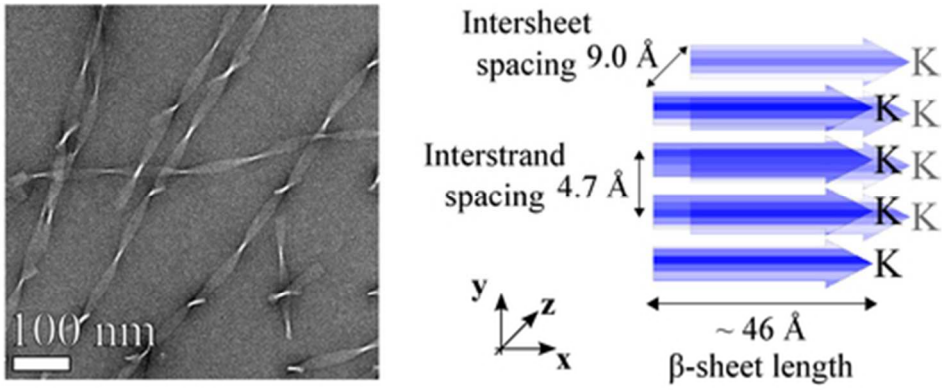

We produce TTR1-based fibrils with a high density of amines for functionalisation following assembly. Fibril assembly is also characterised using a range of solution conditions, including ionic strength.
39x16mm (300 x 300 DPI)